

HD-A132 332

FABRICATION OF A SILICON MOSFET DEVICE WITH BIPOLAR
TRANSISTOR SOURCE(U) HAWAII UNIV AT MANOA HONOLULU DEPT
OF ELECTRICAL ENGINEERING D N OKADA JUL 80

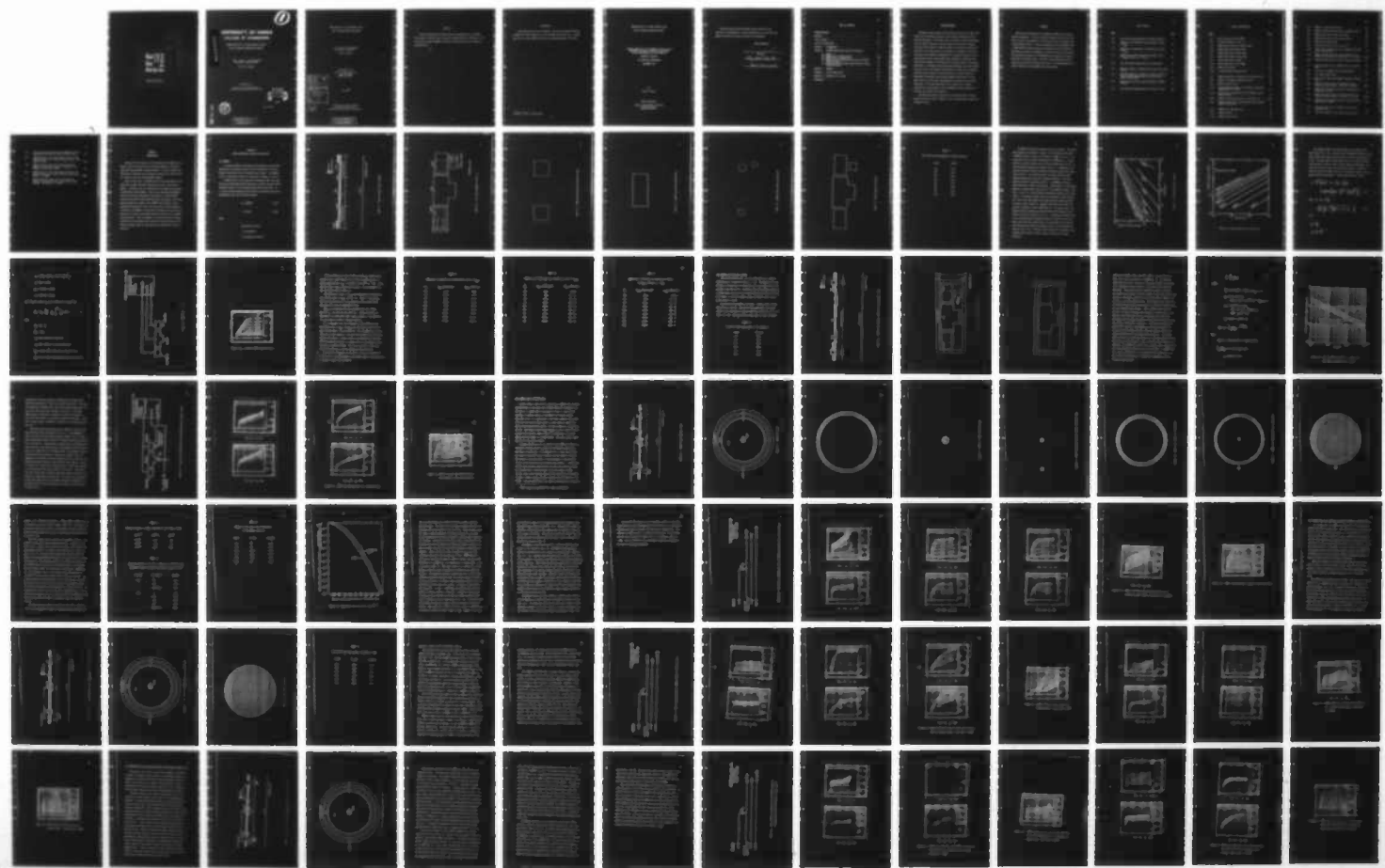
1/2

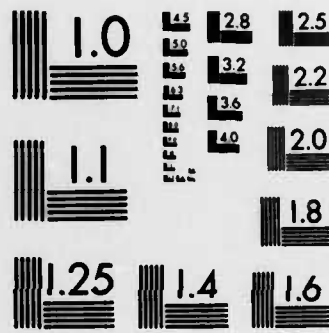
UNCLASSIFIED

N00014-76-C-1081

F/G 9/1

NL





MICROCOPY RESOLUTION TEST CHART
NATIONAL BUREAU OF STANDARDS-1963-A



UNIVERSITY OF HAWAII

COLLEGE OF ENGINEERING

ADA132332

FABRICATION OF A SILICON MOSFET DEVICE
WITH A BIPOLAR TRANSISTOR SOURCE

PROF. JAMES W. HOLM-KENNEDY
PRINCIPAL INVESTIGATOR

DAVID N. OKADA

Sponsored by

Office of Naval Research
under Contract N00014-76-C-1081

DTIC
ELECTED
S D
SEP 13 1983
D

July 1980



DTIC FILE COPY

DISTRIBUTION STATEMENT A
Approved for public release;
Distribution Unlimited

FABRICATION OF A SILICON MOSFET DEVICE
WITH A BIPOLAR TRANSISTOR SOURCE

Prof. James W. Holm-Kennedy
Principal Investigator

David N. Okada

Sponsored by the
Office of Naval Research
under Contract
N00014-76-C-1081

Accession For	
NTIS GRA&I	<input checked="" type="checkbox"/>
DTIC TAB	<input type="checkbox"/>
Unannounced	<input type="checkbox"/>
Justification .	
By Per Ltr. on file	
Distribution/	
Availability Codes	
Dist	Avail and/or Special
A	

July 1980

University of Hawaii at Manoa
College of Engineering
Department of Electrical Engineering



DISTRIBUTION STATEMENT A
Approved for public release
Distribution Unlimited

Abstract

A series of MOS devices evolving the direct integration of a Si MOSFET and a bipolar transistor into a single four terminal device is described. The final device, termed an MOSBJT is shown to exhibit gain and novel electronic characteristics.

Introduction

A novel MOS device has been invented.* The device integrates directly an MOSFET and a BJT resulting in a four terminal device with gain. The MOS gate acts as a high impedance control on the operating region of the BJT.

*Inventor: James W. Holm-Kennedy

FABRICATION OF A SILICON MOSFET DEVICE
WITH A BIPOLAR TRANSISTOR SOURCE

A THESIS SUBMITTED TO THE GRADUATE DIVISION OF THE
UNIVERSITY OF HAWAII IN PARTIAL FULFILLMENT
OF THE REQUIREMENTS FOR THE DEGREE OF

MASTER OF SCIENCE

IN ELECTRICAL ENGINEERING

DECEMBER 1979

By

David N. Okada

Thesis Committee:

James W. Holm-Kennedy, Chairman
Bharat Kinariwala
Kazutoshi Najita

We certify that we have read this thesis and that in our opinion it is satisfactory in scope and quality as a thesis for the degree of Master of Science in Electrical Engineering.

THESIS COMMITTEE

Chairman

Kazutaki Nagita

Bharat Kinawale

TABLE OF CONTENTS

ACKNOWLEDGEMENTS	iv
ABSTRACT	v
LIST OF TABLES	vi
LIST OF ILLUSTRATIONS	vii
CHAPTER 1 INTRODUCTION	1
CHAPTER 2 DEVICE FABRICATION, RESULTS AND ANALYSIS	
2.1 MOSFET	2
2.2 MOSFET with a Bipolar Source	21
2.3 MOSBJT with a Diffused Base	33
2.4 MOSBJT Having an Epitaxial Base and a Diffused Isolation Region	54
2.5 MOSBJT Having an Epitaxial Base and Mesa Etched Isolation Region	70
CHAPTER 3 SUMMARY	83
APPENDIX A DEVICE FABRICATION	85
APPENDIX B PROPERTIES OF SILICON	90
REFERENCES	96

ACKNOWLEDGEMENT

The basic design concept of the devices and the novel ideas incorporated in the devices described in this thesis originated with Dr. James Holm-Kennedy. The author wishes to thank Dr. James Holm-Kennedy for his support, guidance, and many useful clarifying discussions. The author also wishes to thank Paul Saka for his useful discussions and help in the fabrication of the devices, the technical staff consisting of John Johnston, Kamesuke Oshiro, and Melvin Cobb for their conscientious effort toward maintaining, modifying, designing, and fabricating equipment in the University of Hawaii Physical Electronics Laboratory, to Sinthavone Soutavong, Karen Watanabe, and Darrel Motoda for their work in the design and fabrication of the first successful bipolar junction transistor at the University of Hawaii Physical Electronics Laboratory, and to Darrel Motoda and Brian Doi for all their effort in the initial development of the Physical Electronics Laboratory. The author would also like to express his sincere appreciation to Lynn Okumura and Jan Yamamoto for their guidance in preparing and typing the manuscript.

The author and advisor would like to thank the Office of Naval Research for their partial support of this research under Contract No. N 00014-76-C-108.

ABSTRACT

Devices were fabricated that integrated a MOSFET with a bipolar junction transistor. In this new device, minority carriers are injected from the silicon substrate into the base and are collected by the inverted MOSFET channel. Initial investigations were performed using a simple MOSFET structure which was redesigned into a more effective and complex structure (the MOSBJT) to optimize the device performance. The fabrication procedure of the MOSBJT was then modified to improve the bipolar transistor action. The final device performed satisfactorily with a positive transistor gain (β) of ~ 3 and substantial controlled injection into the MOSFET inversion channel.

LIST OF TABLES

Table		Page
1.1	Four point probe measurements of MOSFET Substrate	9
1.2	Comparison of theoretical and experimental values of V_{DSAT}	18
1.3	Comparison of Experimental and theoretical values of I_{DSAT}	19
1.4	Comparison of calculated and experimental values of I_{DSAT} assuming $\mu_n = 0.85 \mu_B$	20
2.1	Four point probe measurements of the substrate . .	21
3.1	Diffusion length vs. doping concentration for p-type silicon	43
3.2	Depletion depth as a function of doping and reverse bias for homogeneously doped, one-sided abrupt planar diode at 300°K.	43
3.3	Results of four point probe measurements of MOSBJT substrate	44
4.1	Four point probe measurements of epitaxial layer. .	58

LIST OF ILLUSTRATIONS

Figure		Page
1.1	Cross Sectional View of MOSFET	3
1.2	Top View of MOSFET of Fig. 1.1	4
1.3	MOSFET Source and Drain Diffusion Mask	5
1.4	MOSFET Gate Oxide Regrowth Mask	6
1.5	MOSFET Metallization Window Mask	7
1.6	MOSFET Metallization Window Mask	8
1.7	Oxide Growth Rate in Steam	11
1.8	Oxide Growth Rate in Dry Oxygen	12
1.9	MOSFET Test Circuit	15
1.10	n-channel MOSFET Characteristics	16
2.1	MOSFET with Bipolar Injection Cross Sectional View	22
2.2	MOSFET with Bipolar Injection Top View	23
2.3	MOSFET Isolation Mask	24
2.4	Surface Depletion Width as a Function of the Doping Concentration in Silicon	27
2.5	Test circuit configuration for the MOSFET Having a Bipolar Source	29
2.6	MOSFET BJT Characteristics as a Function of V_G . .	30-31
2.7	MOSFET "Reverse" BJT Characteristics (Drain-Emitter, Substrate-Collector)	32
3.1	MOSBJT Cross Sectional View	34
3.2	MOSBJT Top View	35
3.3	MOSBJT Isolation Mask	36

3.4	MOSBJT n ⁻ Drain Diffusion Mask	37
3.5	MOSBJT Substrate and Drain Contact Diffusion Mask .	38
3.6	MOSBJT Base Contact and Diffusion Mask	39
3.7	MOSBJT Metallization Contact Window Mask	40
3.8	MOSBJT Metallization Mask	41
3.9	Normalized Curves for erfc α and $e^{-\alpha^2}$	45
3.10	Test Circuit Configuration for the MOSBJT Fabricated with a Diffused Base	49
3.11	MOSBJT (Diffused Base) BJT Characteristics as a Function of Gate Voltage. Gate Oxide is $\sim 10,000\text{\AA}$	50-52
3.12	MOSBJT (Diffused Base) "Reverse" BJT Characteristics	53
4.1	Cross Sectional View of a MOSBJT with an Epitaxial Base	55
4.2	Top View of an MOSBJT with an Epitaxial Base	56
4.3	Gate Oxide Regrowth Mask	57
4.4	Test Circuit Used for the MOSBJT Having an Epitaxial Base	61
4.5	MOSBJT (Epitaxial Base) BJT Characteristics as a Function of Gate Voltage. Gate Oxide is 1200\AA	62-64
4.6	MOSBJT (Epitaxial Base) Reverse BJT Characteristics. Gate Oxide is 1200\AA	65
4.7	MOSBJT (Epitaxial Base) BJT Characteristics as a Function of Gate Voltage. Gate Oxide is $10,000\text{\AA}$	66-68
4.8	MOSBJT (Epitaxial Base) Reverse BJT Characteristics. Gate Oxide is $10,000\text{\AA}$	69
5.1	Cross Sectional View of a MOSBJT with an Etched Isolation Ring	71
5.2	Top View of MOSBJT with an Etched Isolation Ring .	72

5.3	Test Circuit Configuration for the MOSBJT Having an Epitaxial Base and a Mesa Etched Isolation Ring . .	76
5.4	MOSBJT (Epitaxial Base, Mesa Etched Isolation) BJT Characteristics as a Function of Gate Voltage. Gate oxide is 1200 \AA	77-78
5.5	MOSBJT (Epitaxial Base, Mesa Etched Isolation) Reverse BJT Characteristics as a function of Gate Voltage. Gate Oxide is 1200 \AA	79
5.6	MOSBJT (Epitaxial Base, Mesa Etched Isolation) BJT Characterisitcs as a Function of Gate Voltage. Gate Oxide is $\sim 10,000\text{\AA}$	80-81
5.7	MOSBJT (Epitaxial Base, Mesa Etched Isolation) Reverse BJT Characteristics as a function of Gate Voltage. Gate Oxide is $\sim 10,000\text{\AA}$	82

CHAPTER 1

INTRODUCTION

The goal of this project was the integration of a MOSFET with a bipolar junction transistor and to provide substantial controlled injection into the MOSFET inversion channel. This was accomplished with several different device structures and basically involves bipolar injection into the inverted MOSFET channel.

Prior to this effort, no MOSFET had ever been fabricated at the University of Hawaii Physical Electronics Lab (or in the State of Hawaii). Therefore, the first objective was to design and fabricate a conventional silicon MOSFET. After it was confirmed that MOSFETs could be successfully fabricated in the UH lab, the simple MOSFET structure was modified with additional masks and changes in the fabrication procedure to produce a novel MOSFET with a bipolar source. Acceptable performance of these devices justified the development of a new device, the MOSBJT, in which major considerations were given to achieving a net gain and confining current injection into the MOSFET inverted channel. The first MOSBJT (a diffused structure) performed satisfactorily and attempts were then made to achieve device gain by using an epitaxial layer for the base and an etched mesa region for isolation.

CHAPTER 2

DEVICE FABRICATION, RESULTS AND ANALYSIS

2.1 MOSFET

A n-channel MOSFET was designed and fabricated to confirm that MOS devices of acceptable quality could be fabricated in the new Physical Electronics Lab at the University of Hawaii. This MOSFET was of a conventional design as illustrated in Figures 1.1 and 1.2.

A (100) p-type silicon substrate of thickness 0.014" was used. Four point probe measurements were taken at several locations across the wafer (Table 1.1) to characterize the wafer resistivity. A $\sim 1.9 \Omega\text{-cm}$ average substrate resistivity was calculated from the V/I measurements using the following equations:

$$\rho_s' = \frac{\ln 2}{\pi} \frac{V}{I} \quad (1.1)$$

$$\rho = \rho_s'(d) \quad (1.2)$$

where

ρ_s' \equiv sheet resistance

ρ \equiv resistivity

d \equiv substrate thickness .

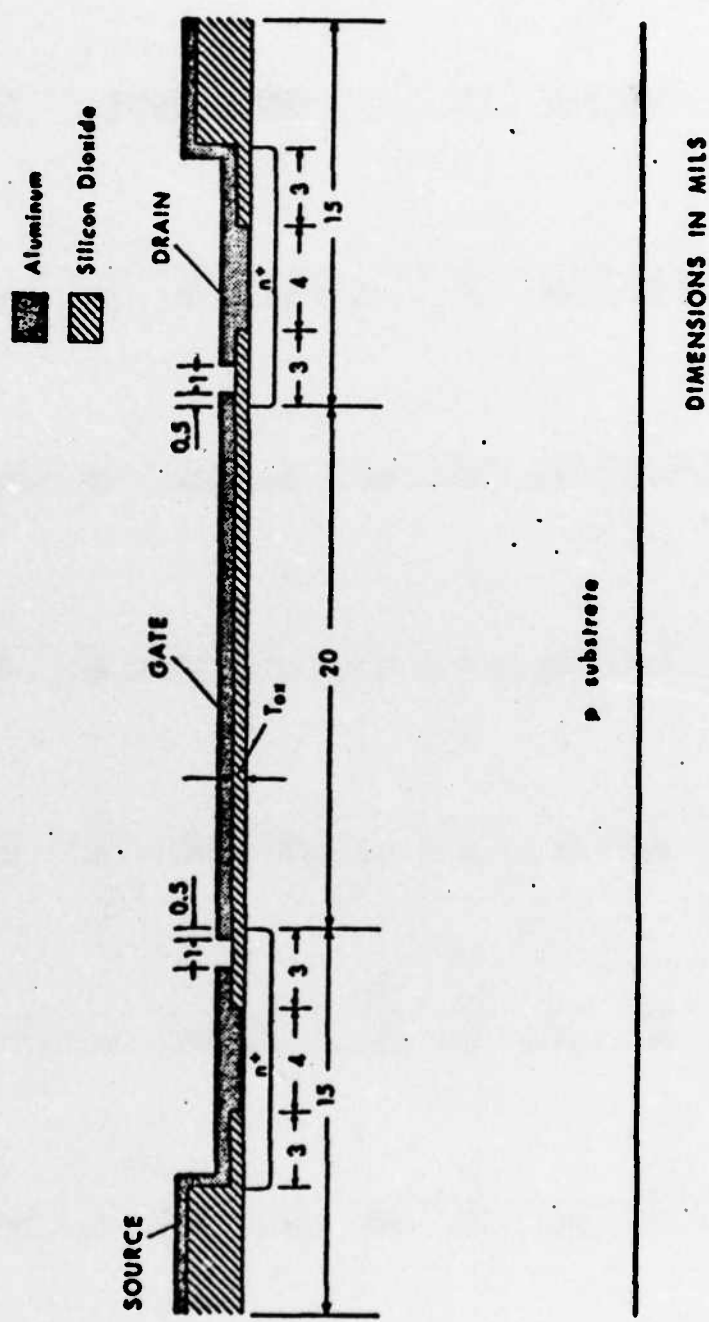


Figure 1.1. Cross sectional view of MOSFET.

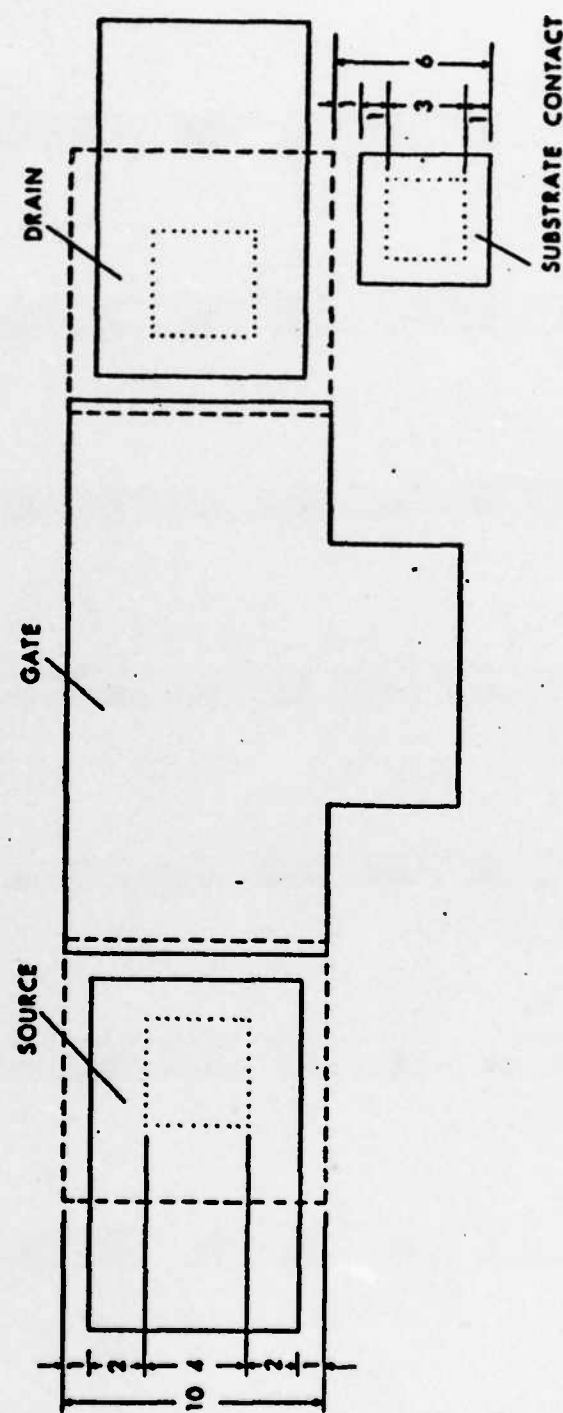


Figure 1.2. Top view of MOSFET of Fig. 1.1.



Figure 1.3. MOSFET source and drain diffusion mask.

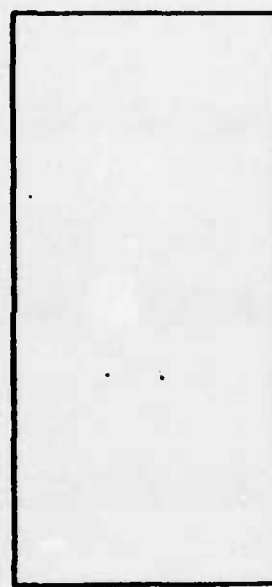


Figure 1.4. MOSFET gate oxide regrowth mask.

Figure 1.5. MOSFET metallization window mask.



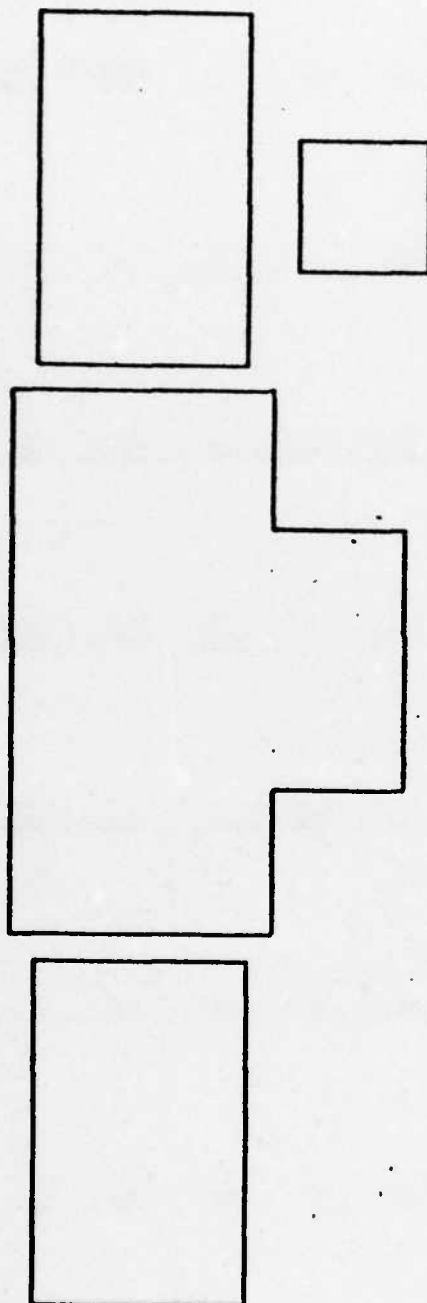


Figure 1.6. MOSFET metallization mask.

TABLE 1.1

Four Point Probe Measurements of MOSFET Substrate

I(μ A)	V/I(Ω)
60	12.0
60	12.3
60	12.3
60	11.5
60	11.9
60	12.0
60	11.9
60	12.3

The MOSFET fabrication procedure used was as follows: The wafers were cleaned using procedure 1 (App. A) and a blocking oxide layer of $\sim 5000\text{\AA}$ was grown in steam for 80 minutes at 1000°C (Fig. 1.7). The oxide color was red violet corresponding to 4600\AA (App. B). Source and drain diffusion windows were cut using the mask shown in Fig. 1.3 and the negative photoresist procedure (App. A). A phosphorous pre-dep was performed at 950°C (15 minutes) followed by P_2O_5 glass removal with dilute HF. The blocking oxide in the gate region was then removed employing the gate oxide regrowth mask (Fig. 1.4) using a negative photoresist procedure (App. A). A 1000\AA gate oxide was grown (100 minute, 1000°C dry oxidation). Oxide growth in a dry oxygen ambient is significantly slower than in a wet oxidation process (see Figs. 1.7 and 1.8) and facilitates reproducible growth of thin oxide layers. A 30 minute nitrogen anneal was performed at 1000°C followed by a "fast pull" (the wafers were removed from the furnace rapidly) to reduce surface states [2]. The gate oxide color was violet confirming a thickness of about 1000\AA (App. B). The source, drain, and substrate contact windows were etched through the blocking and gate oxides using the mask shown in Fig. 1.5. The wafers were then placed into a vacuum system and aluminum deposited at 8×10^{-7} torr for the gate, source and drain contact pads. The metallization was defined using the positive photoresist procedure (App. A) and the metallization mask (Fig. 1.6). The wafers were sintered for 3 minutes at 510°C yielding ohmic contacts to the n^+ source, drain and the p-type substrate.

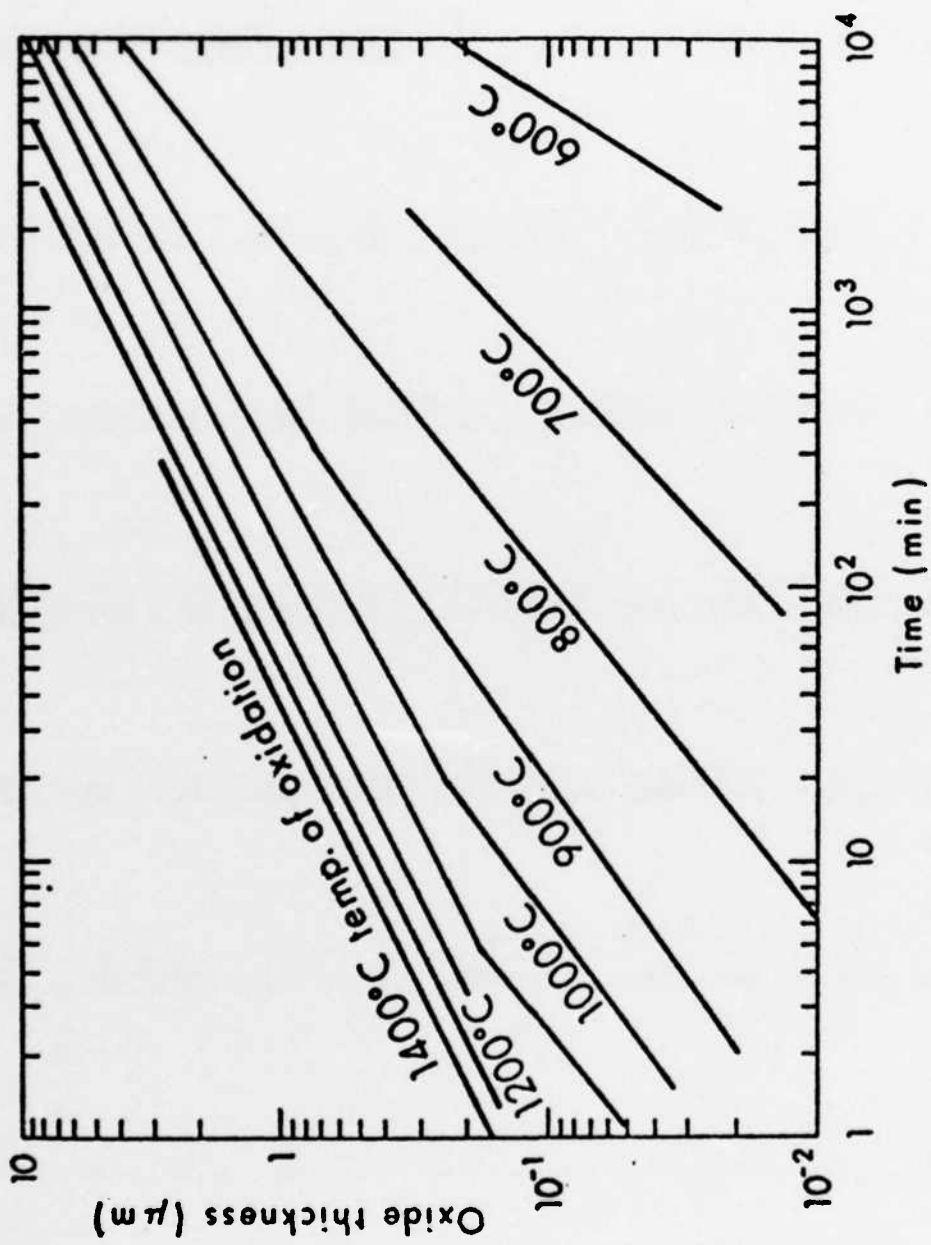


Figure 1.7. Oxide growth rate in steam.¹

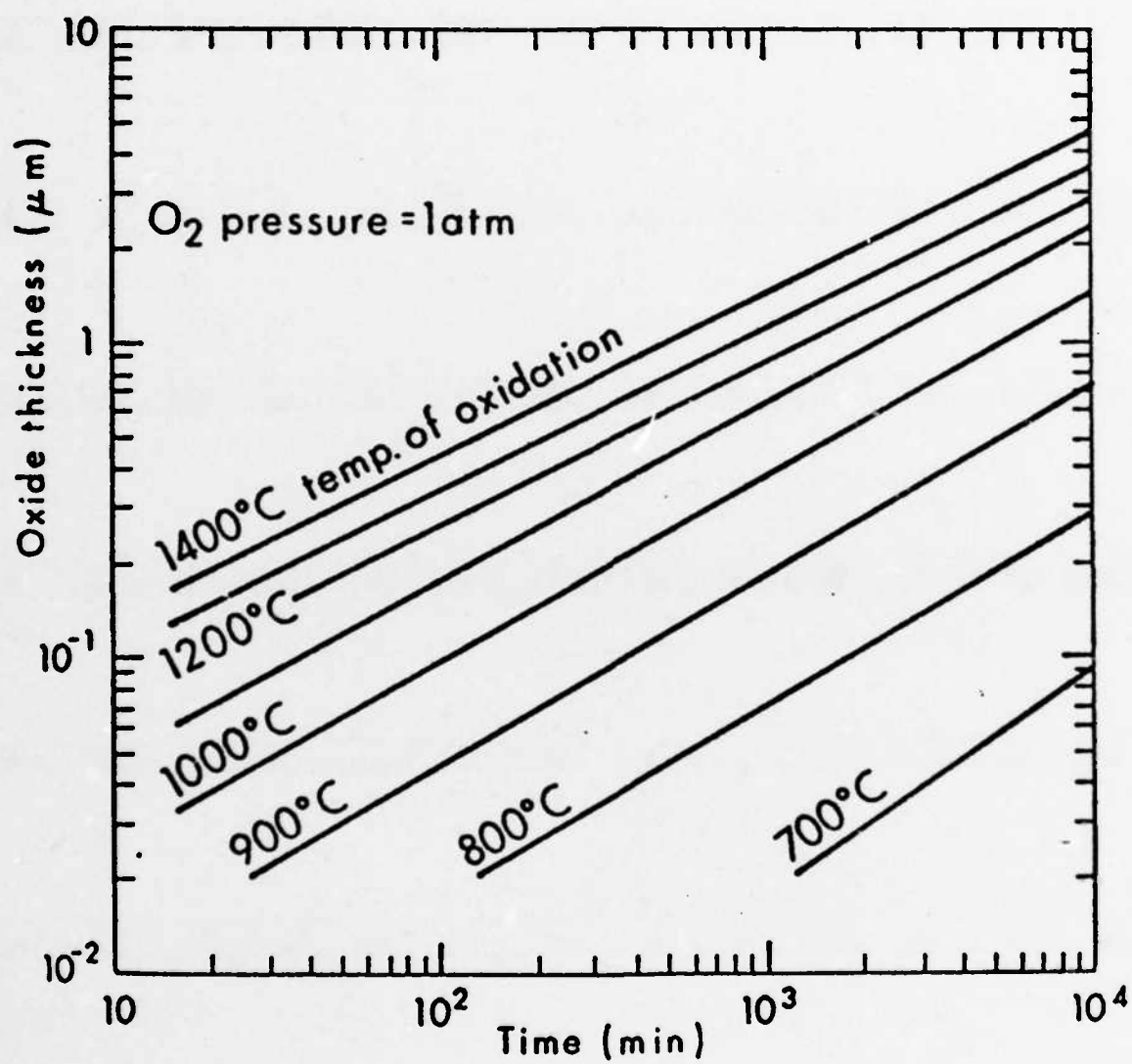


Figure 1.8. Oxide growth rate in dry oxygen¹.

The completed MOSFET was characterized using a Tektronix 576 curve tracer (Fig. 1.9). The curve tracer incremented the gate voltage while measuring the source to drain current versus voltage characteristics. The experimental results shown in Fig. 1.10 can be compared with theoretical source to drain current-voltage relationships. Equations for the drain current and saturation voltage of a MOSFET are derived by Muller and Kamins [6] with a distributed analysis using the gradual-channel approximation. These equations are as follows:

$$I_D = \frac{\mu_n W}{L} \left\{ C_{OX} \left(V_G - V_{FB} - 2|\phi_p| - \frac{1}{2}V_D \right) V_D - \frac{2}{3} \sqrt{2\epsilon_s q Na} \left[\left(2|\phi_p| + V_D \right)^{3/2} - \left(2|\phi_p| \right)^{3/2} \right] \right\} \quad (1.3)$$

$$V_{DSAT} = V_G - V_{FB} - 2|\phi_p| - \frac{\epsilon_s q Na}{C_{OX}} \left[\sqrt{1 + \frac{2C_{OX}}{\epsilon_s q Na} (V_G - V_{FB} - V_B)} - 1 \right] \quad (1.4)$$

where

$$C_{OX} = \frac{\epsilon_{OX}}{x_{OX}}$$

$$\phi_p = \frac{kT}{q} \ln \frac{N_A}{n_i}$$

μ_n = Surface mobility $\approx \frac{1}{2}$ bulk mobility.

V_G \equiv Gate voltage.

V_{FB} \equiv Flat-band voltage.

V_B \equiv Substrate voltage.

The flat-band voltage V_{FB} can be expressed as follows [6]:

$$V_{FB} = \Phi_{MS} - \frac{Q_{SS}}{C_{OX}} - \frac{1}{C_{OX}} \int_0^{X_{OX}} \frac{x}{X_{OX}} \rho(x) dx \quad (1.5)$$

where

$$\Phi_{MS} = \Phi_M - \Phi_S .$$

$$Q_{SS} = q N_{SS} .$$

Φ_M \equiv Work function of the metal.

Φ_S \equiv Work function of the semiconductor.

N_{SS} \equiv Fixed surface state density per unit area.

Q_{SS} \equiv Fixed surface state charge density per unit area.

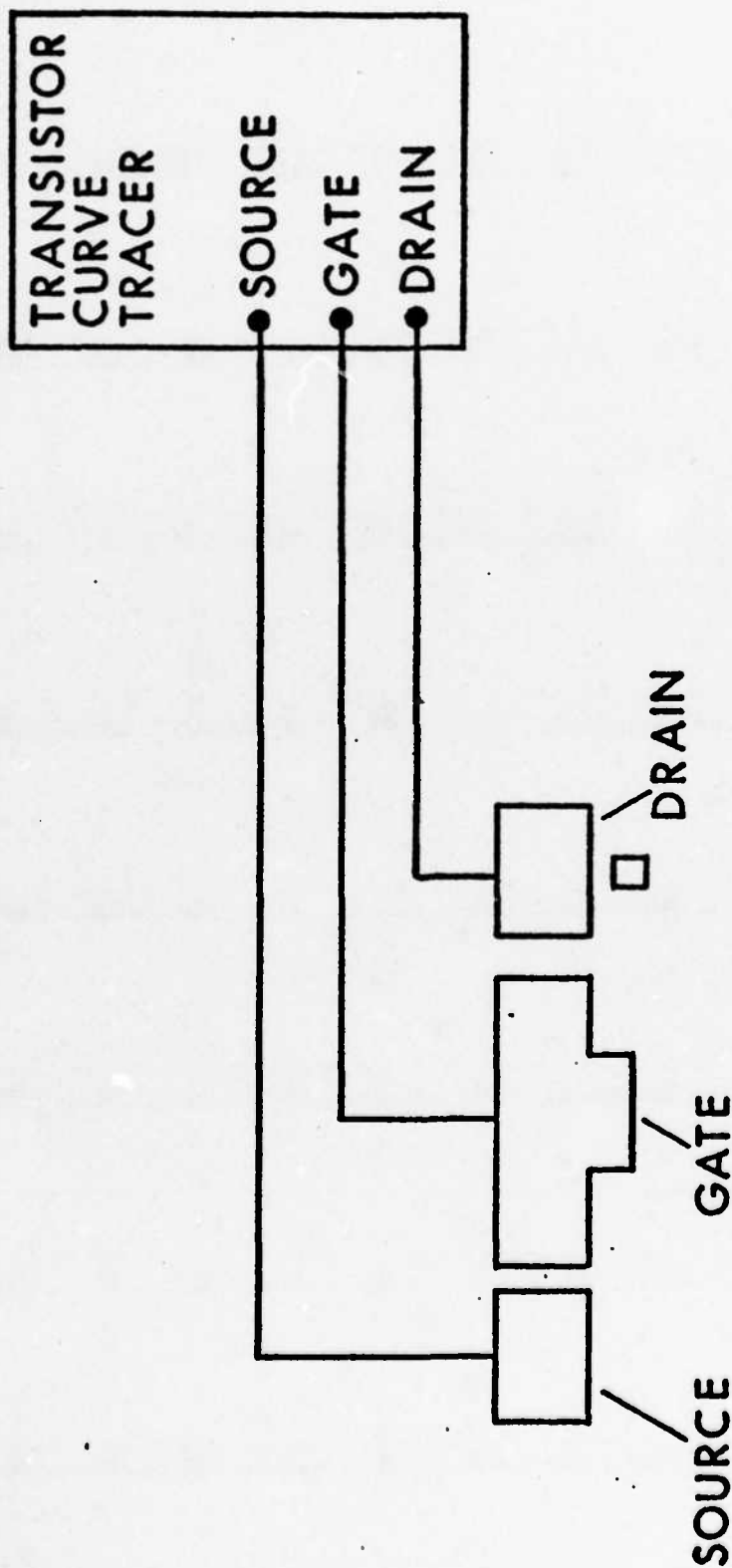
TEXTRONIX TYPE 576

Figure 1.9. MOSFET test circuit.

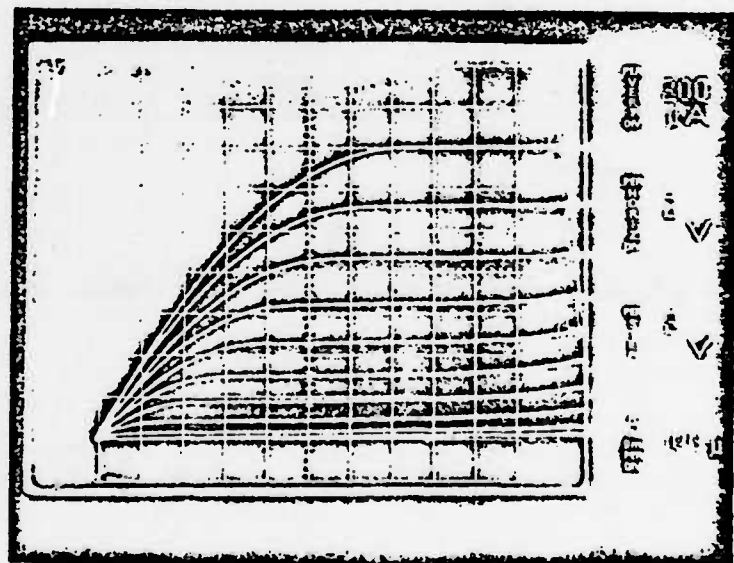


Figure 1.10. n-channel MOSFET characteristics.

In the calculation of the flat-band voltage the integral term resulting from trapped charges in the oxide was neglected and the surface state density, N_{SS} , is assumed to be $8 \times 10^{20} \text{ cm}^{-2}$ [2]. Theoretical values of V_{DSAT} calculated using Eq. 1.4 are compared with the experimental data in Table 1.2.

The theoretical values of I_{DSAT} were determined by substituting the computed values of V_{DSAT} into Eq. 1.3. Table 1.3 illustrates that the calculated values of the saturation drain current agree reasonably well with the experimental data.

I_{DSAT} was calculated with the assumption that the surface mobility, μ_n , was half the bulk mobility. A better agreement of experimental and theoretical data, shown in Table 1.4, was obtained if μ_n was taken to be 85% of the bulk mobility.

It is improbable that the difference in the theoretical and experimental data of I_{DSAT} and V_{DSAT} was the result of the surface mobility being 85% of the bulk mobility. The discrepancies are more likely due to the fringing of the gate field increasing the effective width of the channel, a larger surface state density than expected, nonuniform substrate doping, or slight errors in the values of oxide thickness or substrate doping. The latter could not be more accurately confirmed due to lack of appropriate test equipment.

Satisfactory performance of the MOSFET justified proceeding to the next step in the development of the MOSBJT, namely the introduction of a bipolar source into the MOSFET.

TABLE 1.2

Comparison of theoretical and experimental values of V_{DSAT}

V_G	V_{DSAT} Experimental	V_{DSAT} Theoretical
2V	1.5V	0.82V
4V	2.7V	2.1 V
6V	4.3V	3.6 V
8V	6.0V	5.1 V
10V	7.4V	6.6 V
12V	9.2V	8.2 V
14V	11.0V	9.8 V
16V	12.5V	11.5 V
18V	14.5V	13.1 V

TABLE 1.3

Comparison of experimental and theoretical values of I_{DSAT}

V_G	I_{DSAT} Experimental	I_{DSAT} Theoretical
2V	20 μA	4.5 μA
4V	70 μA	29 μA
6V	150 μA	76 μA
8V	280 μA	148 μA
10V	420 μA	247 μA
12V	610 μA	371 μA
14V	820 μA	524 μA
16V	1070 μA	703 μA
18V	1400 μA	910 μA

TABLE 1.4

Comparison of calculated and experimental values

of I_{DSAT} assuming $\mu_n = .85\mu_B$

V_G	I_{DSAT} Experimental	I_{DSAT} Theoretical
2V	20 μA	6.9 μA
4V	70 μA	45 μA
6V	150 μA	117 μA
8V	280 μA	227 μA
10V	420 μA	380 μA
12V	610 μA	570 μA
14V	820 μA	806 μA
16V	1070 μA	1080 μA
18V	1400 μA	1400 μA

2.2 MOSFET with a Bipolar Source

The previous MOSFET (Sec. 2.1) was fabricated in a p region diffused into a n substrate (Figs. 2.1, 2.2). The approach was used because of relative ease of fabrication and to test the initial integration of the BJT and FET. Forward biasing the substrate (emitter)/p region (base) junction, while reverse biasing the inversion channel with respect to the base region provides the MOSFET with a distributed "bipolar" source.

The fabrication proceeded as follows. A (100) n-type silicon substrate was selected. Four point probe measurements were made (Table 2.1) to determine an average substrate resistivity of $5.1 \Omega\text{-cm}$ (Eqs. 1.1, 1.2). The wafers were cleaned (App. A) and a 80 minute

TABLE 2.1
Four point probe measurements of the substrate

I (mA)	V/I (Ω)
1.0	20.1
1.0	23.7
1.0	20.5
1.0	24.6
1.0	21.0
1.0	24.8

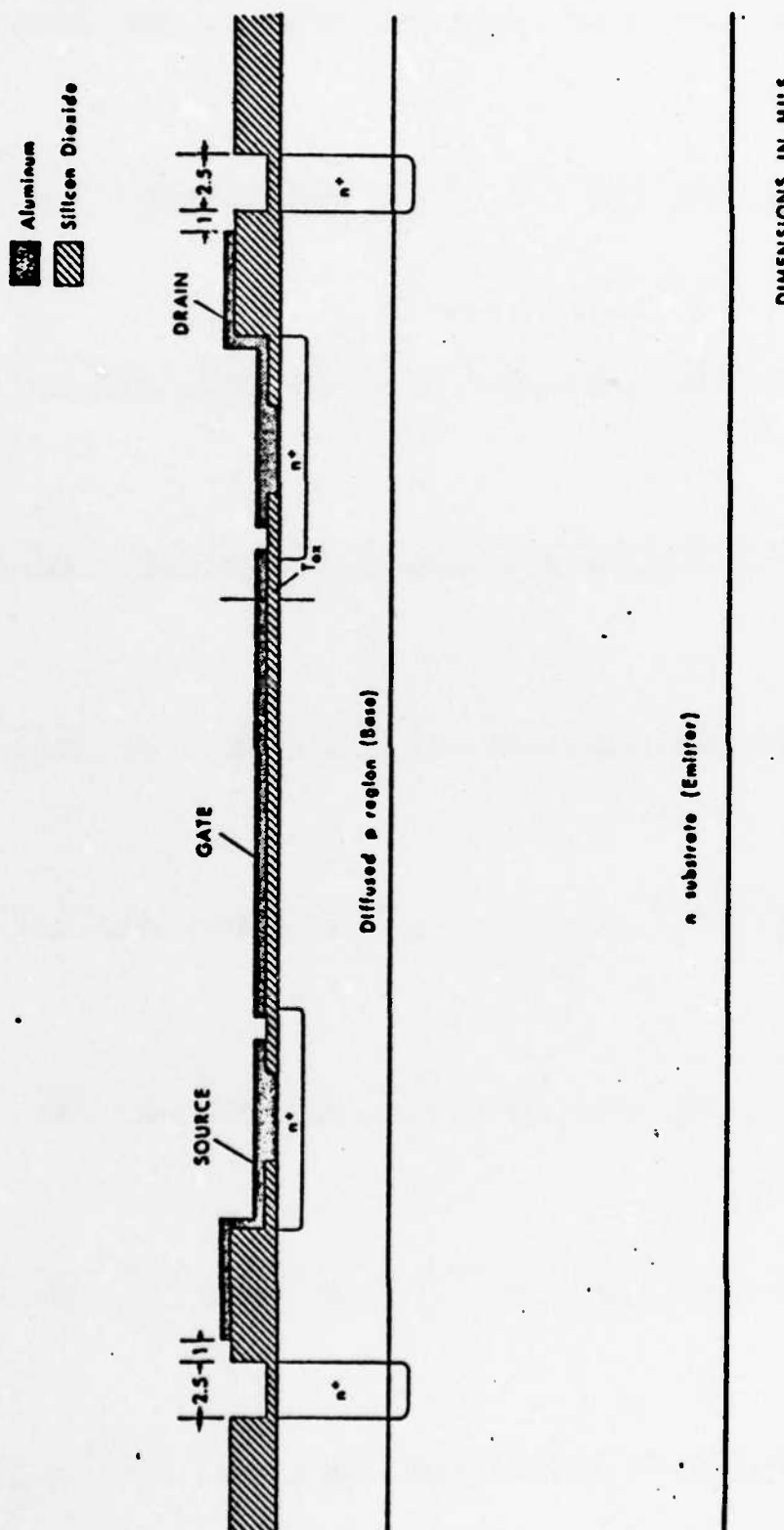


Figure 2.1. MOSFET with bipolar injection cross sectional view.

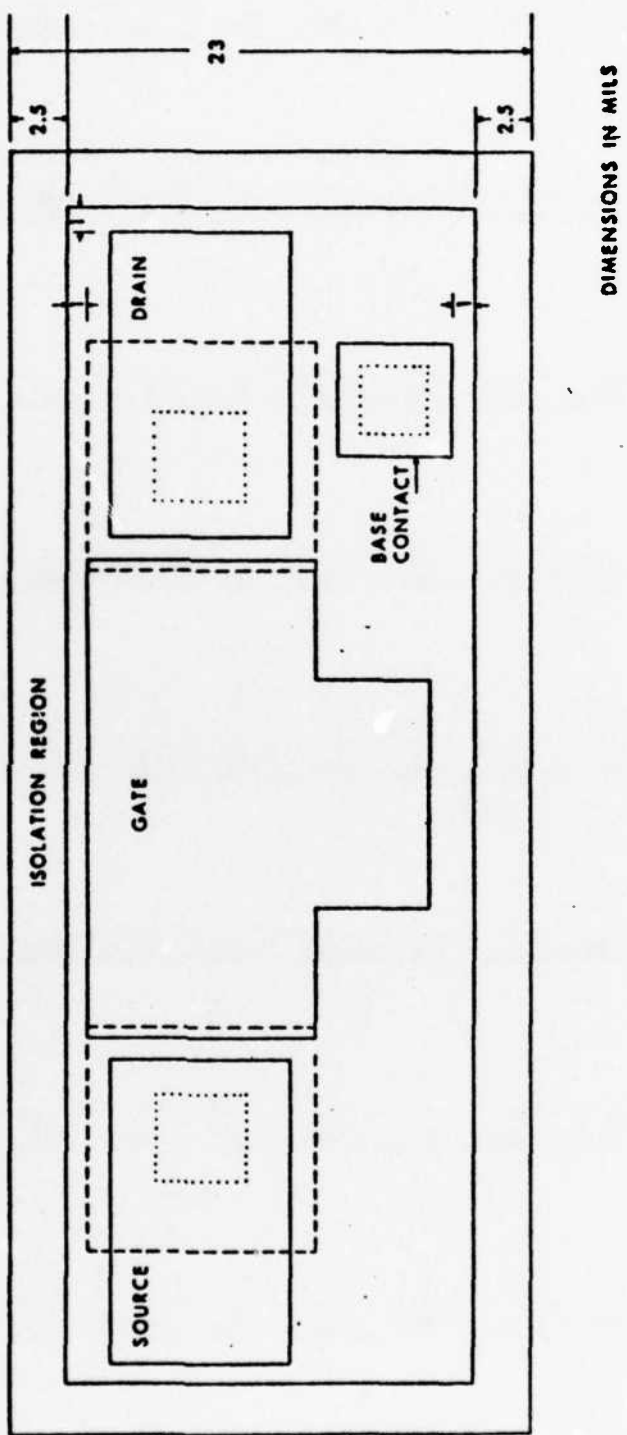


Figure 2.2. MOSFET with bipolar injection top view.

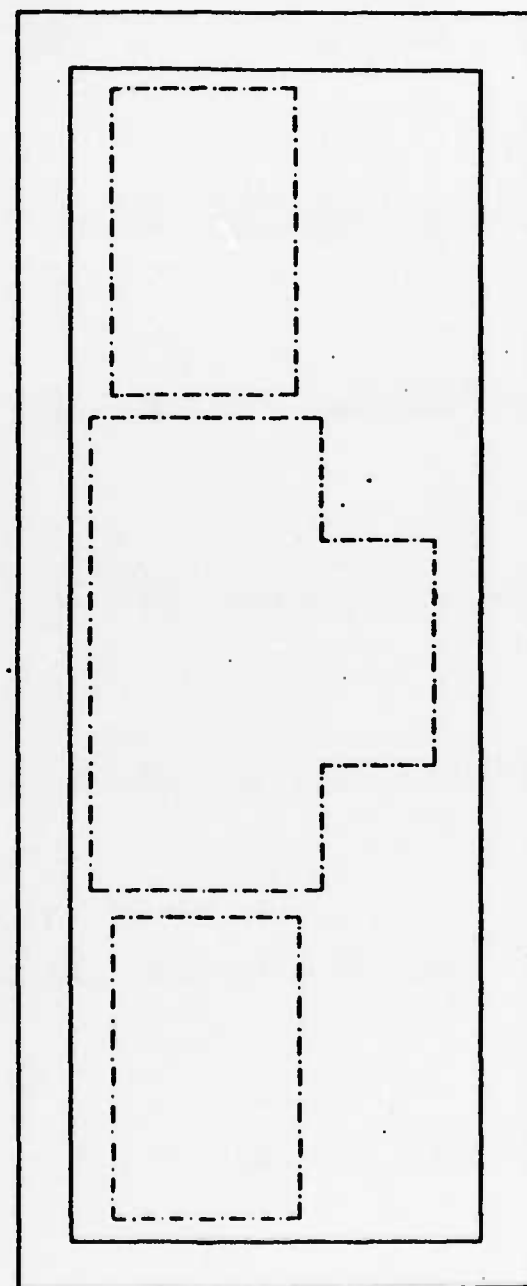


Figure 2.3. MOSFET isolation mask.

1000°C wet oxidation process performed (Table 1.2), resulting in a blue violet oxide corresponding to 4800 \AA (App. B). The blocking oxide layer was left on the back of the wafer to prevent the doping of the substrate contact (the back of the wafer) during the base diffusion. This was achieved by protecting the back of the wafer with negative photoresist during the removal of the oxide on the front surface of the wafer. Operation of the FET/BJT device imposes constraints on the base doping profile. The diffused p-layer must have a sufficiently low surface concentration to allow the inversion layer to form at modest gate voltages. Since a lighter doping profile results in a deeper depletion into the base at inversion (Fig. 2.4), the base width should be of sufficient thickness to prevent the drain/base junction depletion region from extending through the base but should be narrow for a large gain. To achieve the appropriate base profile a 750°C 15 minute predep was performed followed by a dilute HF etch to remove the B_2O_3 glass and therefore reduce the surface concentration of the final diffusion profile. The predep layer was driven at 1150°C for 6 hours in a dry oxygen ambient during the first hour and 45 minutes to grow a blocking oxide preventing out diffusion, in nitrogen for 3 hours and 41 minutes, and in steam during the final 34 minutes to increase the oxide thickness to $\sim 6000\text{\AA}$ (Fig. 1.3). This procedure led to a calculated junction depth of 3.7 μm and a surface concentration of $3.2 \times 10^{16} \text{ cm}^{-3}$ determined from the following equations [4]:

$$\frac{Q}{A} = \frac{2N_0}{\sqrt{\pi}} \sqrt{D_B t_B} \quad (2.1)$$

where

$\frac{Q}{A}$ ≡ Total number of impurity atoms per area.

N_0 ≡ Solid solubility.

Boron at 725C $2.2 \times 10^{20} \text{ cm}^{-3}$ (Appendix B).

D_B ≡ Diffusivity of Boron.

725C $10^{-7} \mu^2/\text{h}$ (Appendix B)

1100C $1.6 \times 10^{-1} \mu^2/\text{h}$

t_B ≡ Length of predep; and

$$N_A(x, t_d) = \frac{Q}{A} \frac{1}{\sqrt{\pi D_B t_d}} e^{-x^2/4D_B t_d} \quad (2.2)$$

where

$N_A(x, t_d)$ ≡ Doping profile of impurity atoms.

$\frac{Q}{A} \frac{1}{\sqrt{\pi D_B t_d}}$ ≡ Surface concentration.

t_d ≡ Length of drive.

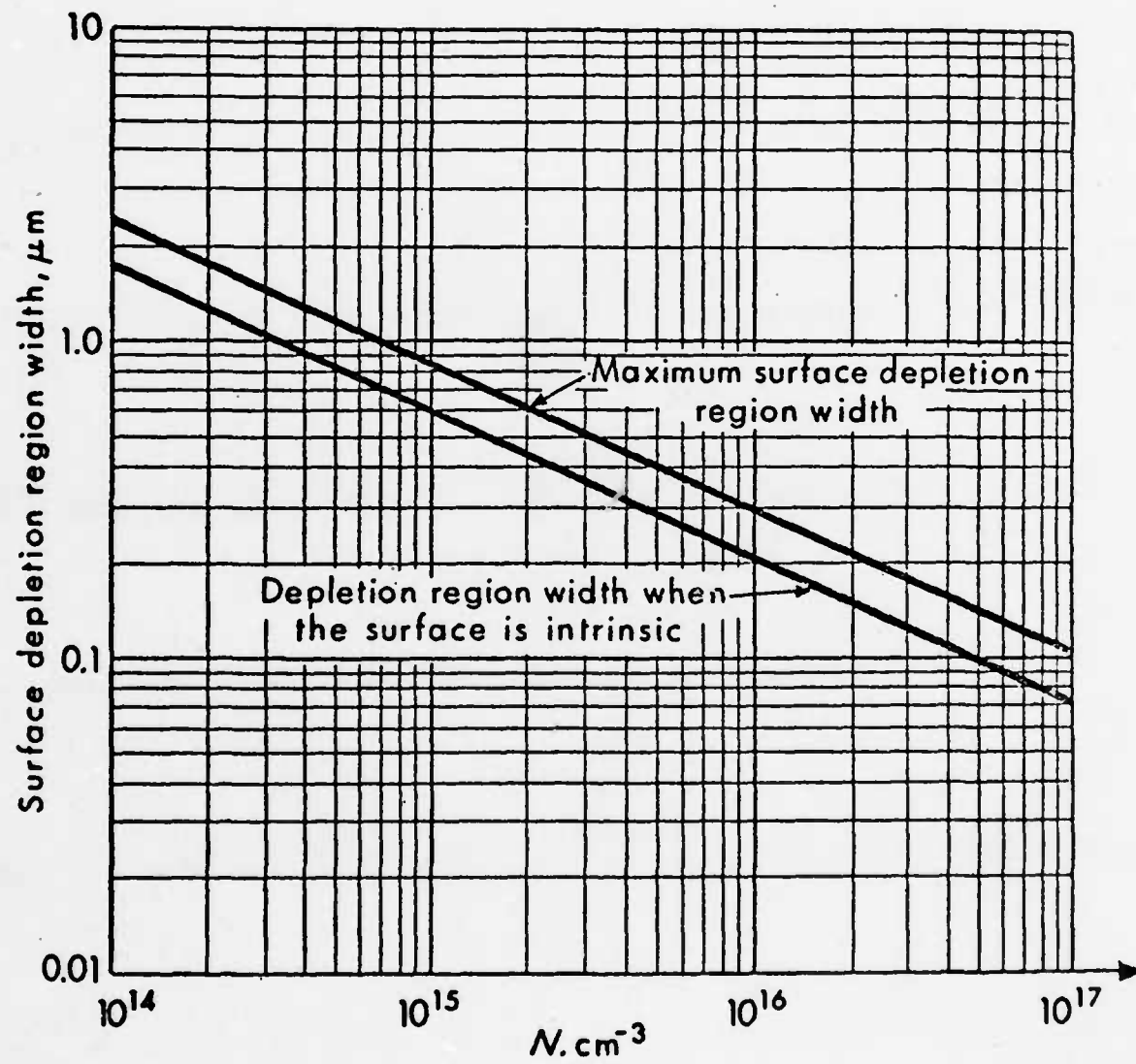


Figure 2.4. Surface depletion width as a function of the doping concentration in silicon.³

A phosphorous diffusion designed to compensate the diffused base profile was performed to electrically isolate the devices. The negative photoresist procedure (App. A) and the isolation mask (Fig. 2.3) was used to define and etch a window in the oxide. A 30 minute 1000C predep was performed, followed by a dilute HF etch and a 3 hour drive during which a dry oxide was grown for 20 minutes. Within this isolation region, the MOSFET of Chapter 2.1 was fabricated (see Fig. 2.2).

The devices were characterized using a Tektronix Type 576 curve tracer and the circuit illustrated in Fig. 2.5. The dependence of bipolar transistor characteristics on gate voltage (Fig. 2.6) reveal that increased gate voltage results in increased collector current and gain of the device. Increased gate voltage results in the enhancement of the inversion layer density and as a consequence channel saturation occurs at a larger value of collector current. The observed increase in gain when the gate voltage is increased is probably due to the dependence of the current collecting capability of the inversion layer (without saturation effects) on the inversion layer density. Figure 2.7 displays the "reverse" BJT characteristics, in which the substrate is the collector and the drain contact is the emitter. The substantial gain results from a favorable drain/base junction injection efficiency and a significant collector area. The effect gate voltage had on the BJT characteristics confirmed the successful integration of a BJT and FET and it was then appropriate to proceed to the next level of device design.

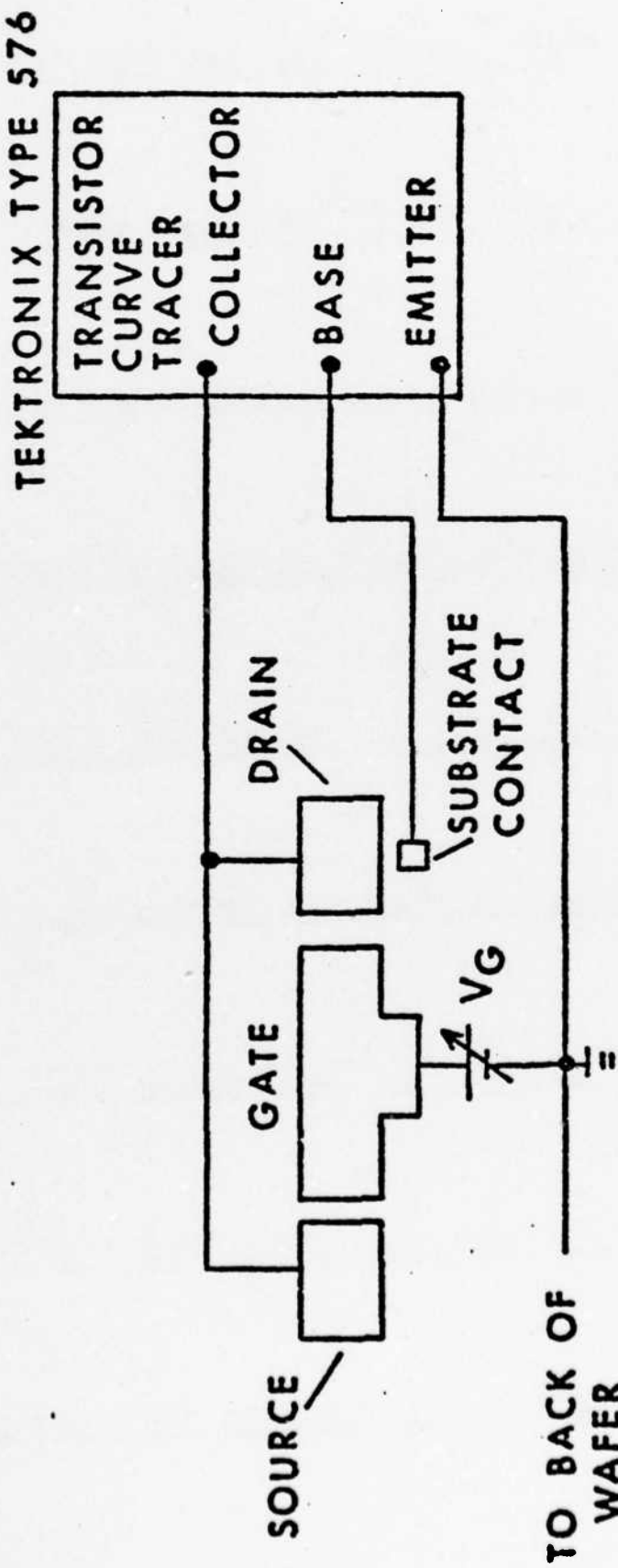


Figure 2.5. Test circuit configuration for the MOSFET having a bipolar source.

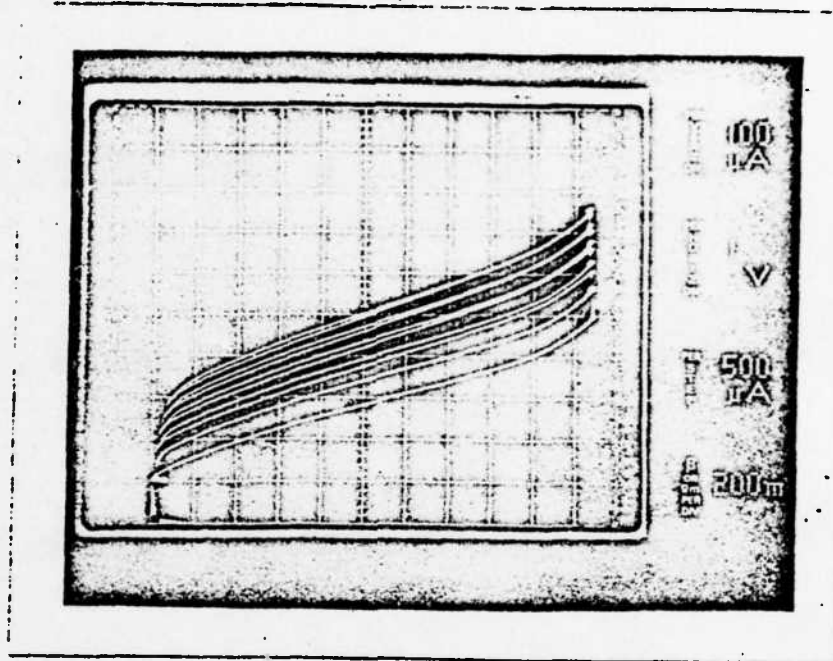


Fig. 2.6a. $V_G = 0V$

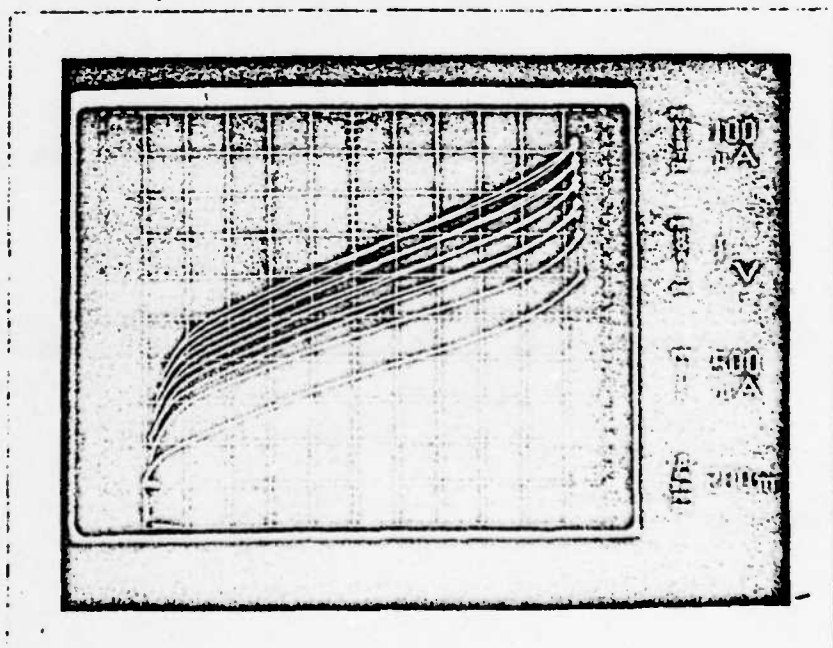


Fig. 2.6b. $V_G = 10V$

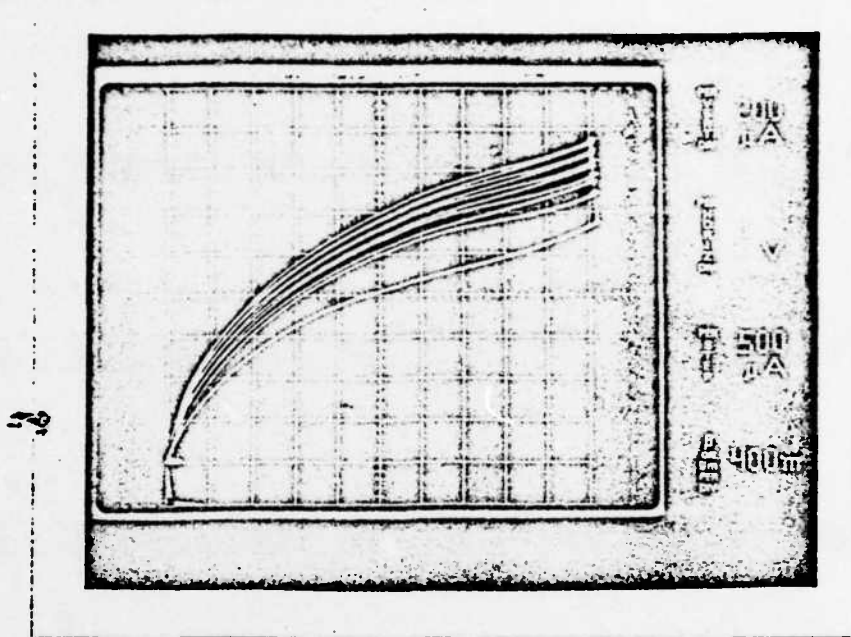


Fig. 2.6c. $V_G = 15V$

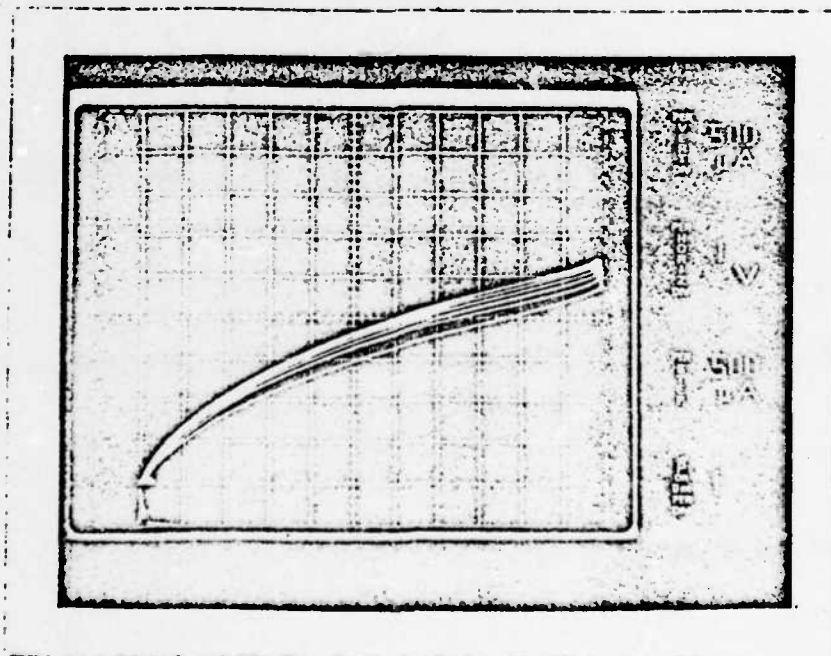


Fig. 2.6d. $V_G = 20V$

Figure 2.6. MOSFET BJT characteristics as a function of V_G .

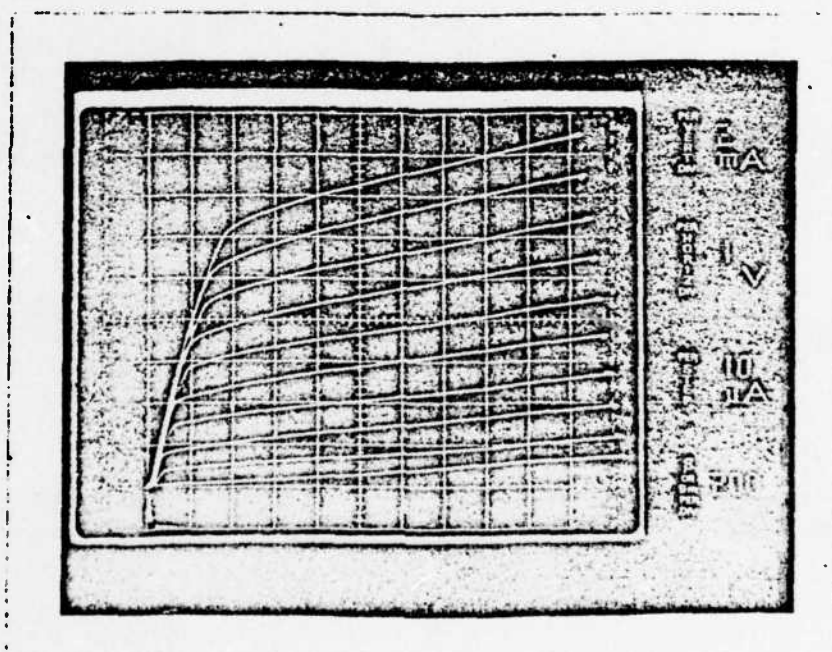


Figure 2.7. MOSFET "reverse" BJT characteristics.
(Drain-Emitter, Substrate-Collector)

2.3 MOSBJT with a Diffused Base

A novel device, which will be called here a MOSBJT, was designed¹ and fabricated in the University of Hawaii Physical Electronics Lab. The device is schematically represented in Figs. 3.1 and 3.2 and operates in a manner similar to the MOSFET with bipolar source described in Sec. 2.2, except that it provides a geometry consistent with the final device target, which is a MOS inversion mode device with a distributed bipolar source. The device operates in the following way: the forward biased substrate/base junction injects minority carriers into the base, some of which is collected by the reverse biased inverted channel of the MOS device. Thus, here the BJT takes the place of the source contact.

A major consideration in the design of the MOSBJT was given to a structure confining the BJT injection to the MOSFET channel while providing a net BJT gain. To accomplish this a large circular gate was chosen to minimize current crowding, provide symmetry, increase the collector area, and assist in the confinement of the injected current to the vicinity of the collector (MOS channel). A large gain requires that the base width be much less than the diffusion length. On the other hand a limiting factor to the base width is punch through, which occurs when the base depletion (resulting from applied voltages) extends through the base. Further, the performance of the MOSBJT is strongly dependent on the impurity concentration in the base

¹Basic design was provided by Dr. James Holm-Kennedy.

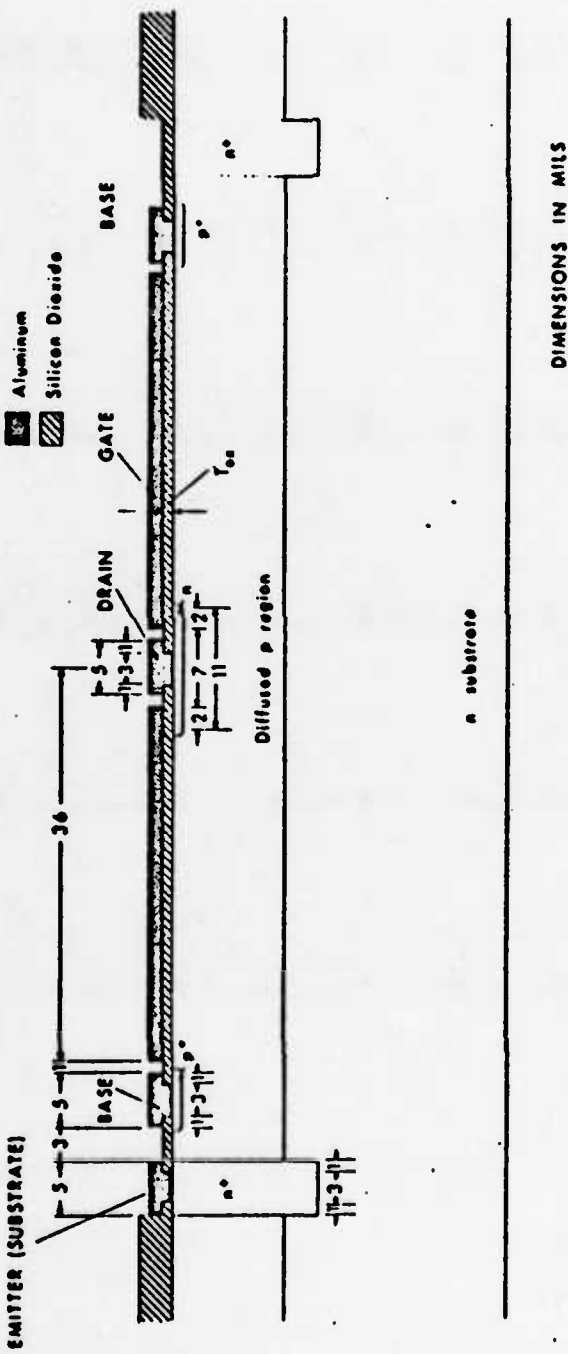


Figure 3.1. MOSBJT cross sectional view.

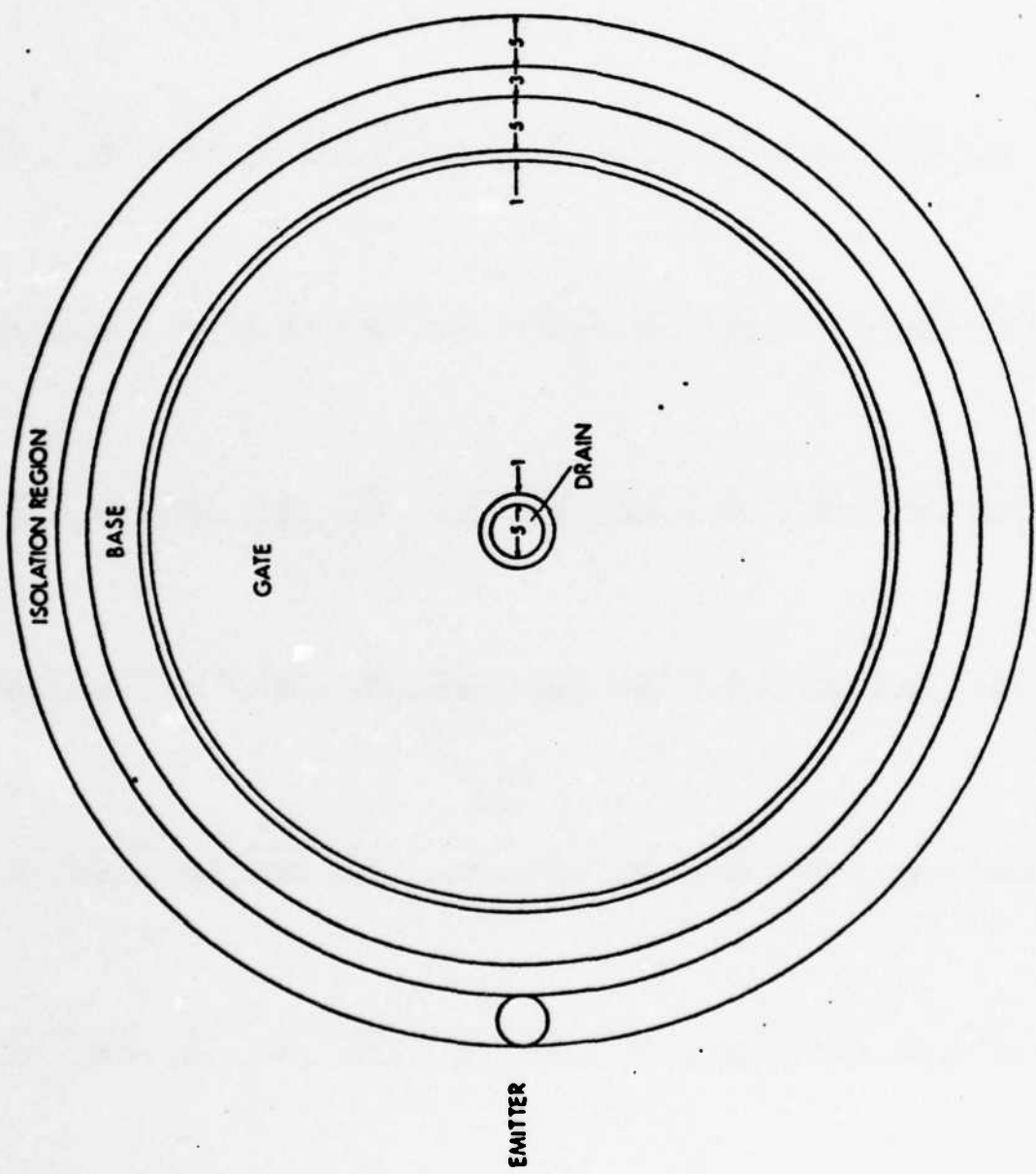


Figure 3.2. MOSBJT top view.

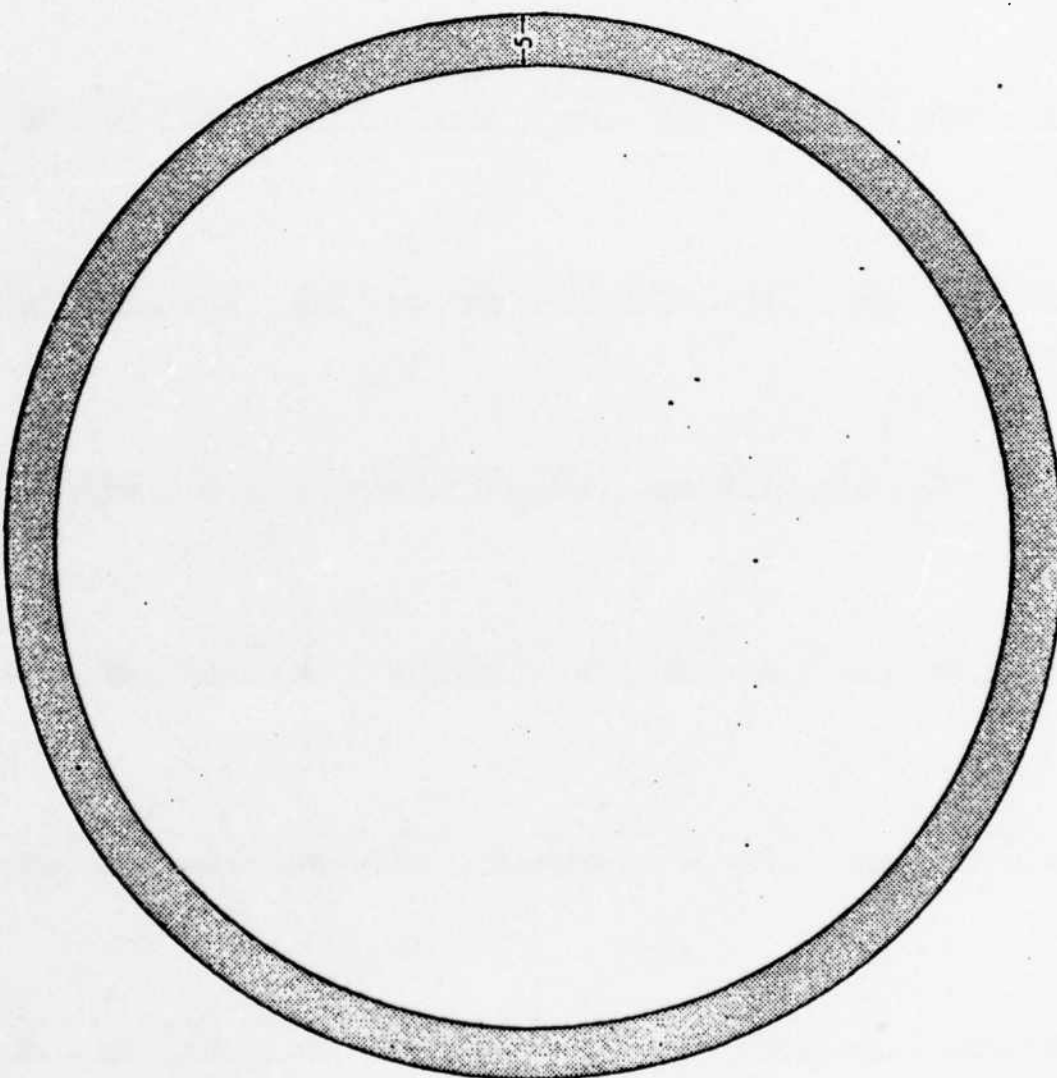


Figure 3.3. MOSBJT isolation mask.

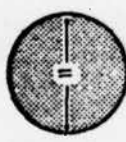


Figure 3.4. MOSBJT n^- drain diffusion mask.

Figure 3.5. MOSBJT substrate and drain contact diffusion mask.



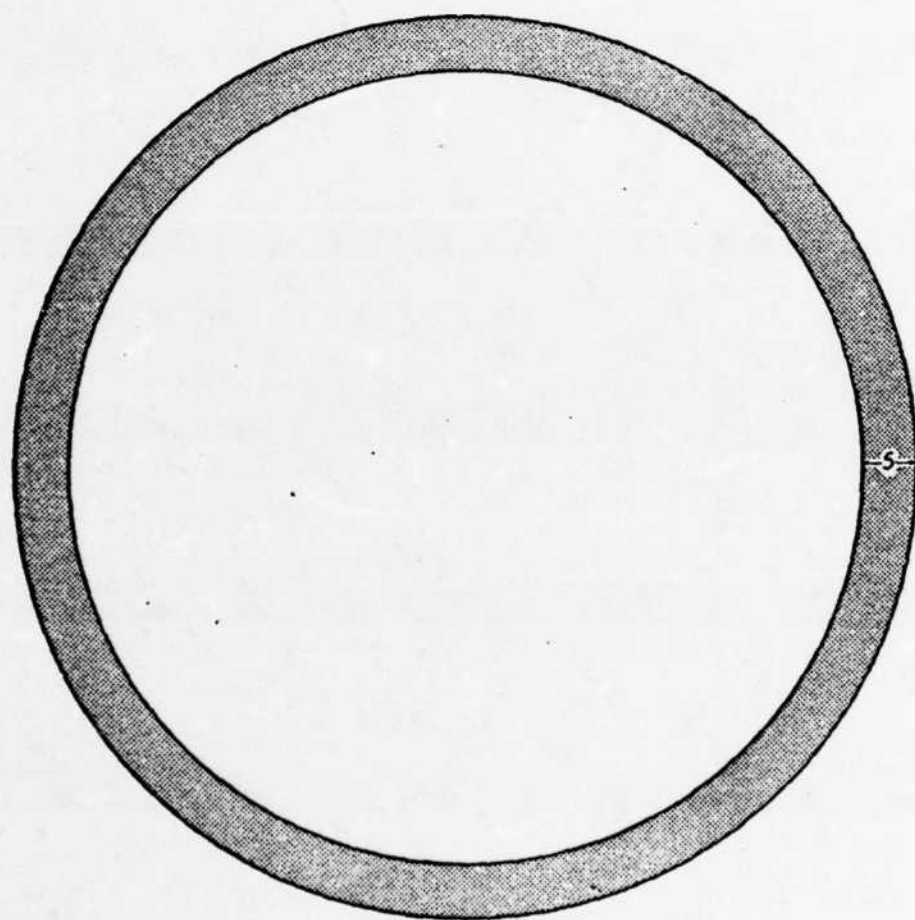


Figure 3.6. MOSBJT base contact and diffusion mask.

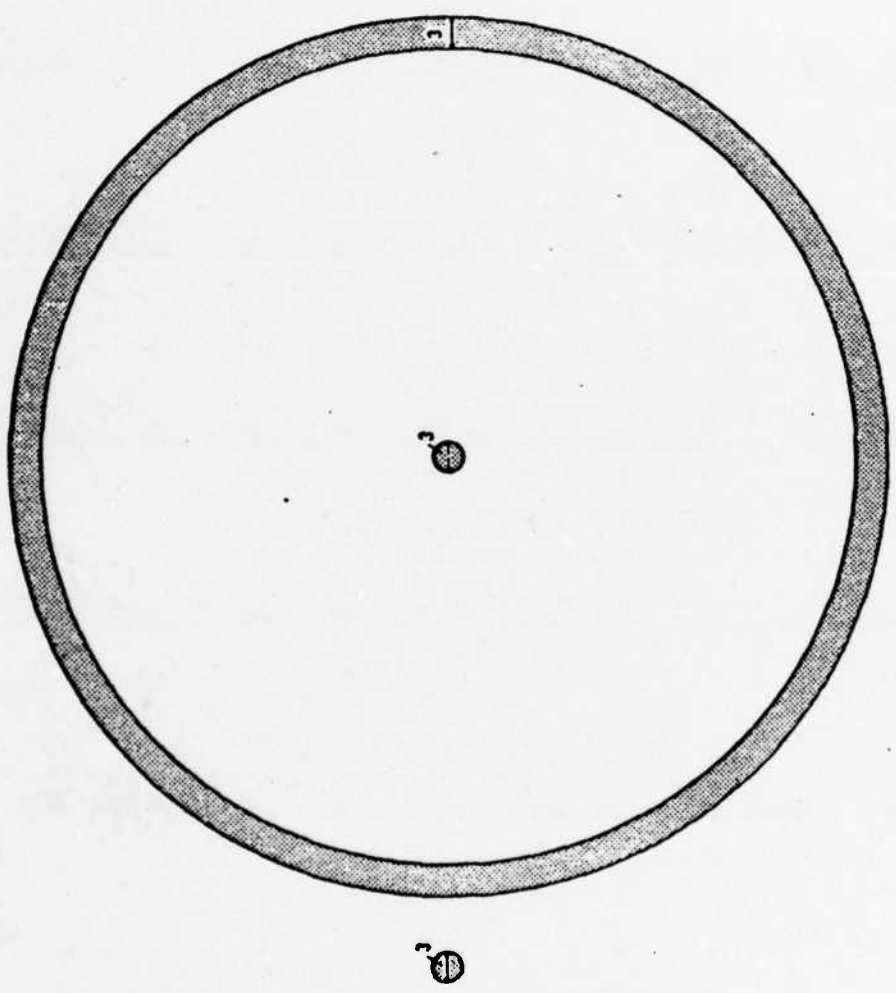


Figure 3.7. MOSBJT metallization contact window mask.

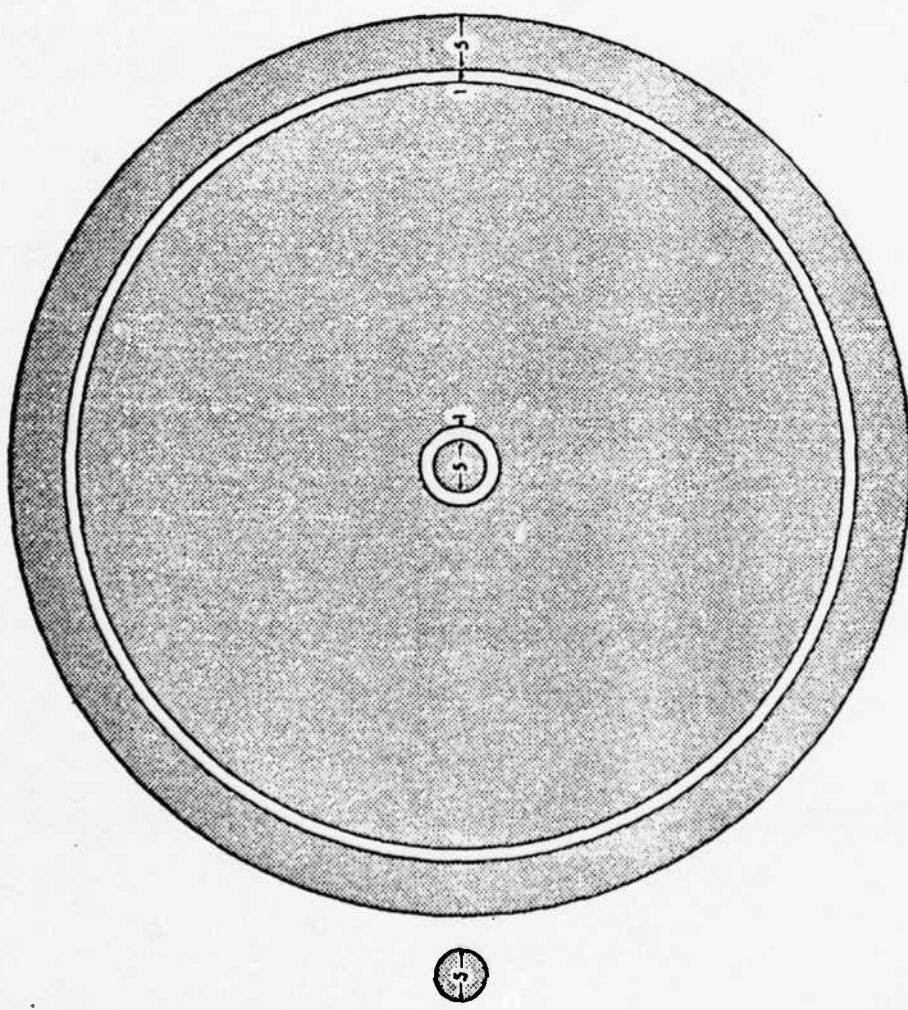


Figure 3.8. MOSJF metallization mask.

region. For a large gain one desires a lightly doped, narrow base and a long minority carrier diffusion length (Table 3.1). The resistivity of the base region also controls the drain/base breakdown voltage and depletion depth (Table 3.2) as well as the depletion into the base due to V_g (Fig. 2.4).

The device fabrication and processing proceeded as follows. Consistent with the above device design constraints, a (100) 2-4 $\Omega\text{-cm}$, 0.013" thick, n-type silicon substrate was chosen. Four point probe measurements (Table 3.3) revealed its resistivity to be $\sim 2.8 \Omega\text{-cm}$ (Eqs. 2.4, 2.5). The wafers were cleaned (App. A) and a 750C, 30 minute boron predep performed followed by a dilute HF etch to remove the B_2O_3 glass. The predep was driven in at 1150C for 19 hours in a wet oxygen ambient during the first 45 minutes and in dry nitrogen for the remaining time. The result was a violet oxide $\sim 4600\text{\AA}$ (App. B). This procedure led to a calculated surface concentration of $7.6 \times 10^{16} \text{ cm}^{-3}$ and a junction depth of 6.9 μm (Eq. 2.1 and 2.2). The negative photoresist procedure (App. A) was used with the isolation mask (Fig. 3.3) to create a circular window in the blocking oxide. The following phosphorous predep yielded a erfc impurity profile. The normalized erfc curve (Fig. 3.9) was used to determine that a 2.7 hour 1100C process would result in an impurity profile that compensates the base impurity profile forming the isolation region and substrate contact.

The drain contact diffusion consisted of two steps. First an initial light phosphorous predep was performed before the gate oxide

TABLE 3.1

Diffusion length vs. doping concentration for p-type silicon⁵

$N_A \text{ cm}^{-3}$	$\rho (\Omega\text{-cm})$	$L_n (\mu\text{m})$
5×10^{17}	0.1	46
2×10^{16}	1.0	79
1×10^{15}	10.0	155

TABLE 3.2

Depletion depth as a function of doping and reverse bias for homogeneous doped, one-sided abrupt planar diode at 300°K⁶

$\rho (\Omega\text{-cm})$	V_R (Volts)	$x_d (\mu\text{m})$
0.1	10	1.0
	20	1.2
	45 (B.D.)	2.0
1.0	1	1.0
	10	3.0
	30	5.0
	90	9.0
	200 (B.D.)	10.6

TABLE 3.3
Results of four point probe measurements
of the MOSBJT substrate

I (mA)	V/I (Ω)	ρ ($\Omega\text{-cm}$)
1.0	19	2.8
1.0	19	2.8
1.0	19.5	2.9
1.0	19.5	2.9
1.0	19.5	2.9
1.0	19	2.8

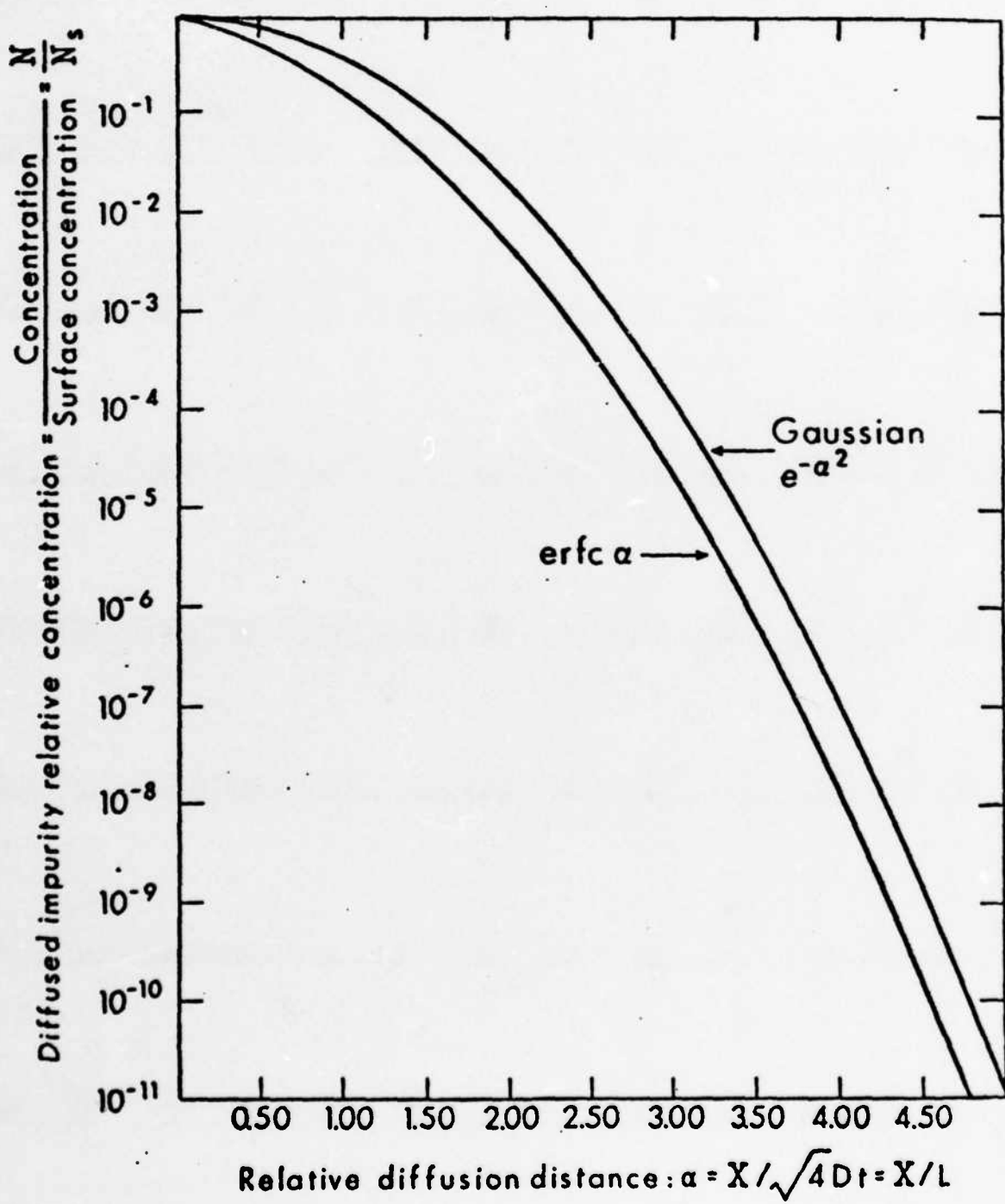


Figure 3.9. Normalized curves for $\text{erfc } \alpha$ and $e^{-\alpha^2}$.

thus ensuring overlap and resultant electrical contact with the inversion layer. The predep was kept light to suppress and limit its diffusion during the growth of the gate oxide. After the gate oxide was grown, a heavy phosphorous predep was performed to raise the surface concentration thereby guaranteeing a quality ohmic connection to the drain. To accomplish this, the n^- drain diffusion mask (Fig. 3.4) was used with the negative photoresist procedure to define and open a window in the SiO_2 for the light phosphorous predep (800°C, 30 minutes). After a dilute HF etch to remove the P_2O_5 layer the remaining oxide color over the gate was violet $\sim 3000\text{\AA}$ (App. B). A two hour wet oxidation followed at 1100°C to increase the gate oxide thickness to $\sim 10,000\text{\AA}$ (Fig. 1.3) resulting in a violet oxide $\sim 1.05 \mu\text{m}$ or $0.86 \mu\text{m}$ (App. B). (The thick oxide was to provide for a homogeneous conduction channel thickness at relatively high injection current.) The substrate and drain contact mask (Fig. 3.5) was used (negative photoresist procedure App. A) to define and etch windows in the SiO_2 followed by a 15 minute, 950°C phosphorous predep for the n^+ substrate and drain electrical contact. A dilute HF etch removed the P_2O_5 glass. A violet $\sim 1000\text{\AA}$ (App. B) blocking oxide was then grown (15 minutes, 1000°C wet oxidation). A window in the SiO_2 for the base contact diffusion was defined and etched (negative photoresist procedure) using the mask shown in Fig. 3.6. A 15 minute 950°C boron predep was then performed to improve the quality of the base contact. After B_2O_3 glass removal (dilute HF etch) a $\sim 1000\text{\AA}$ blocking oxide was grown (15 minute, 1000°C, wet O_2). Windows in the SiO_2

were defined and open with the negative photoresist procedure using the metallization contact mask (Fig. 3.7). These windows provide for electrical contact between the aluminum and the substrate, base, and drain contact diffusions. Aluminum was evaporated at 8×10^{-7} torr and was defined with the metallization mask (Fig. 3.8) and the positive photoresist procedure (App. A).

The MOSBJT was characterized using a Tektronix Type 576 curve tracer as illustrated in Fig. 3.10. The MOSBJT bipolar junction transistor characteristics as a function of gate voltage is shown in Fig. 3.11. For a constant gate voltage and base current, the collector current gradually increases as the collector (drain)-emitter (substrate) voltage increases. This effect was much more pronounced at large gate voltages and probably results from the collection of electron-hole pairs generated in the reverse biased drain/base junction and in the depletion region under the gate. Increases in gate voltage or drain to emitter voltage enlarges the depletion region volume and therefore increases the total number of electron-hole pairs thermally generated in this volume and therefore the number of electrons collected by the reverse biased inversion layer and drain contact thereby resulting in an increased collector current.

The MOSBJT bipolar junction transistor characteristics reveals a similar dependence on gate voltage as the MOSFET with bipolar source (Sec. 1.2). The device gain and value at which the collector current saturates increases as the gate voltage is increased, probably due to the increase in the inversion layer density (discussed in Sec. 1.2).

The maximum BJT gain of ~ 0.8 is probably a result of low injection efficiency (substrate/base junction) resulting from a graded base concentration which is greater than the emitter concentration. The reverse BJT characteristics (in which the substrate is the collector and the drain the emitter) shown in Fig. 3.12 displayed a gain of ~ 200 . This is consistent with a favorable injection efficiency of the emitter (drain)/base junction.

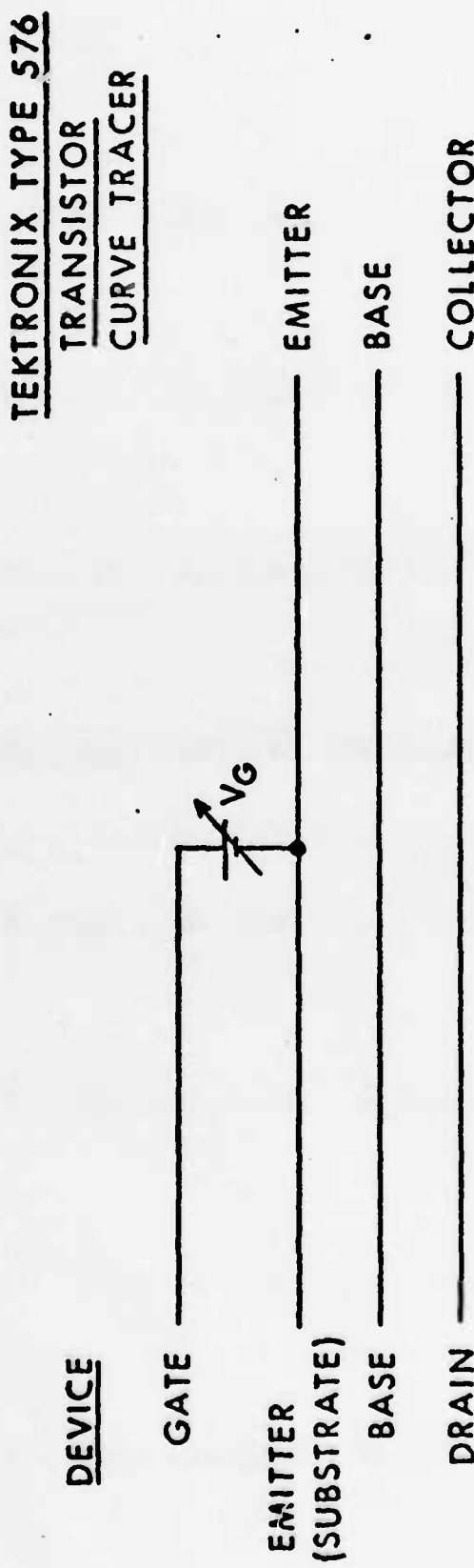


Figure 3.10. Test circuit configuration for the MOSBJT fabricated with a diffused base.

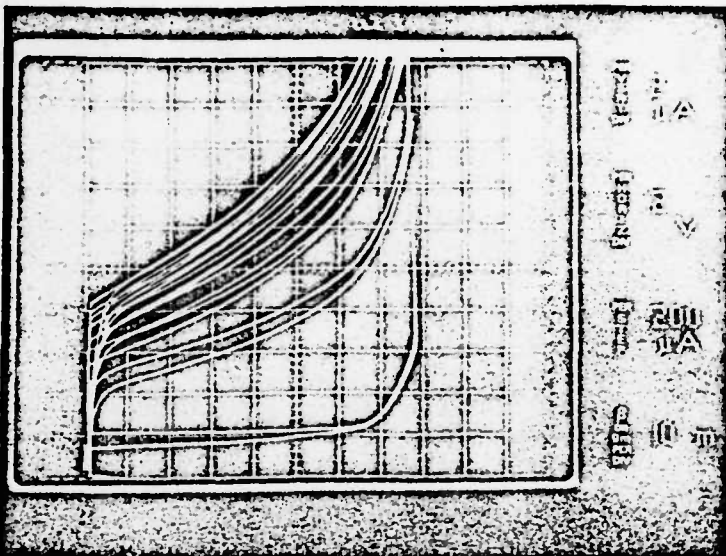


Fig. 3.11a. $V_G = -10V$

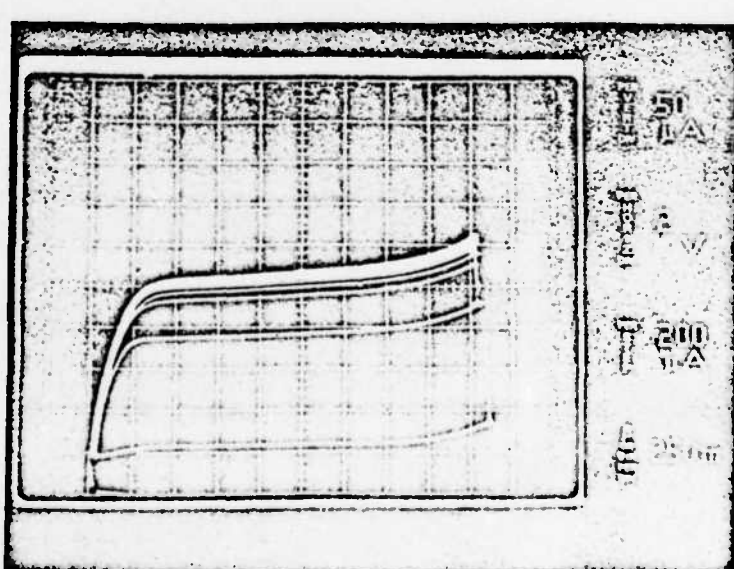


Fig. 3.11b. $V_G = +10V$

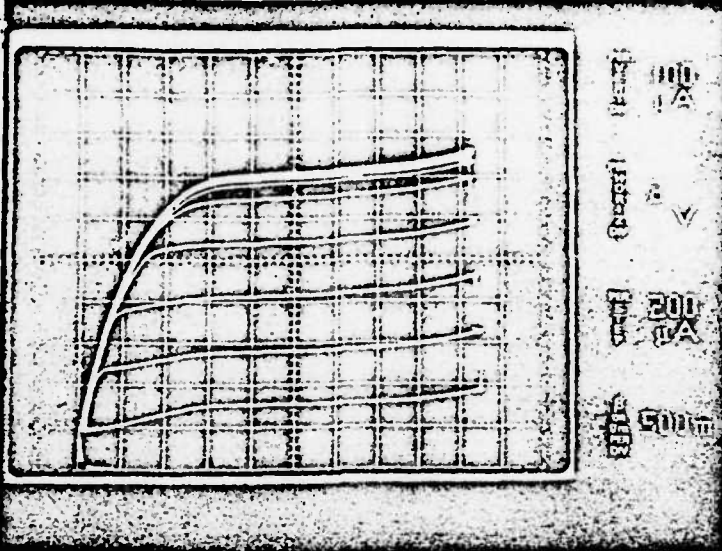


Fig. 3.11c. $V_G = 20V$

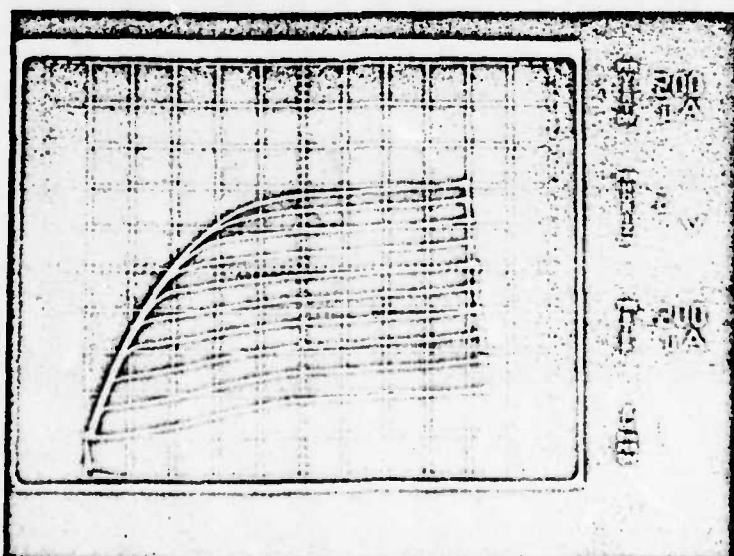


Fig. 3.11d. $V_G = 30V$

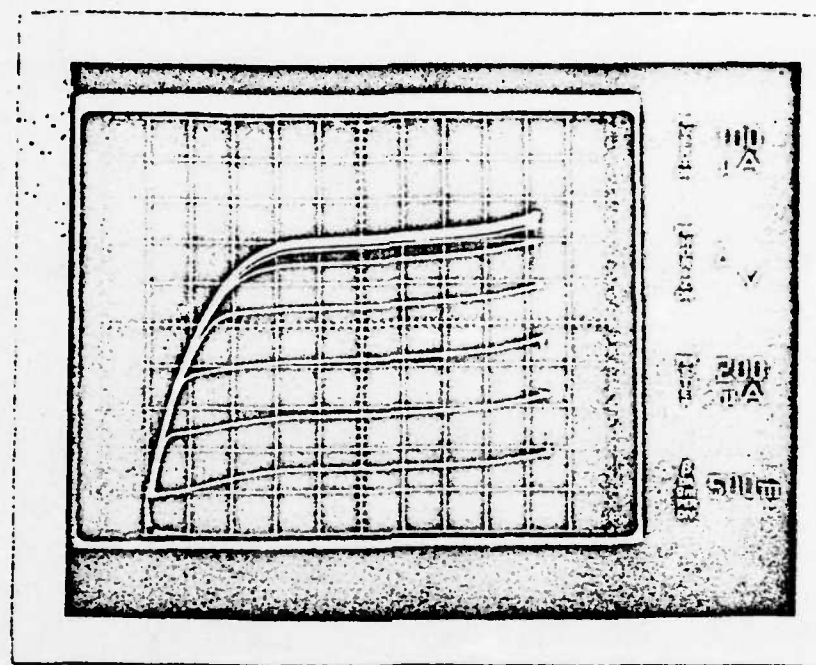


Fig. 3.11c. $V_G = 20V$

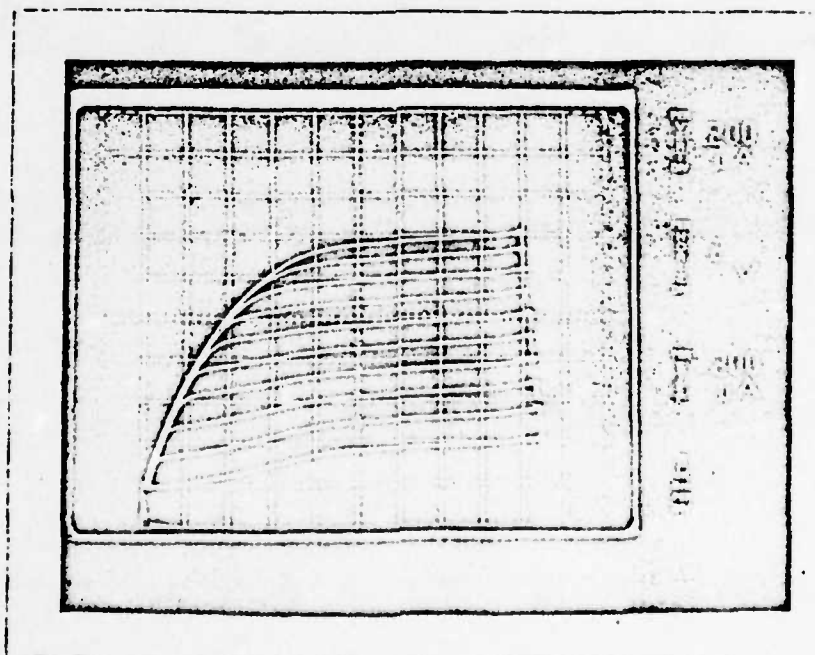


Fig. 3.11d. $V_G = 30V$

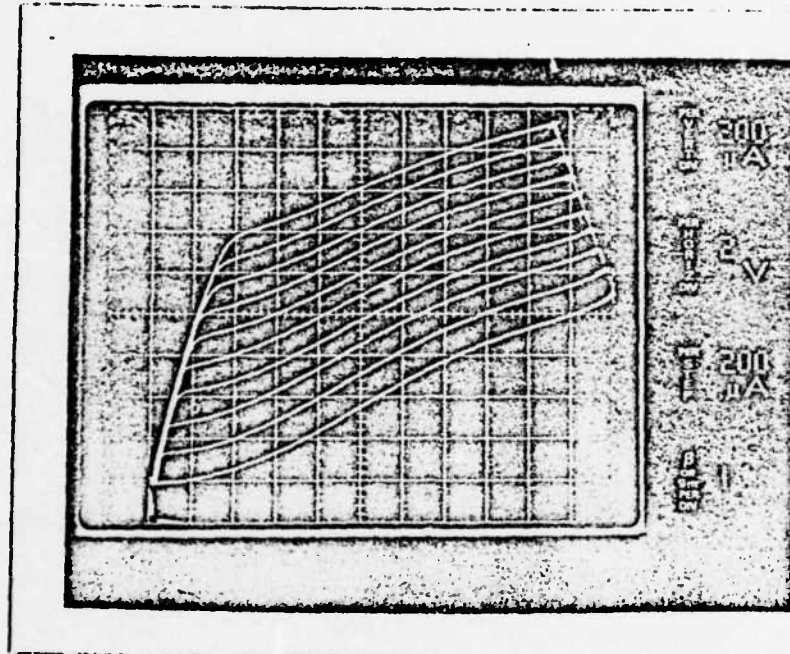


Fig. 3.11e. $V_G = 50V$

Figure 3.11. MOSBJT (diffused base) BJT characteristics as a function of gate voltage. Gate oxide is $\sim 10,000\text{A}^{\circ}$.

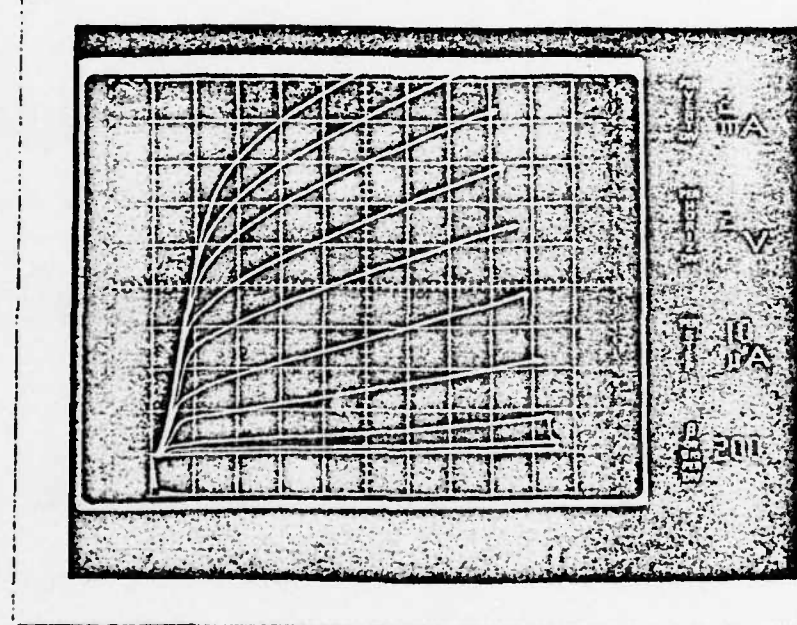


Figure 3.12. MOSBJT (diffused base) "reverse" BJT characteristics.

2.4 MOSBJT Having an Epitaxial Base and a Diffused Isolation Region

To provide gain in an MOSBJT, consideration of a concentration design constraint was necessary. This constraint was met by growing a $10 \mu\text{m}$, $1 \Omega\text{-cm}$ p-type epitaxial layer on a n^+ substrate (Fig. 4.1) in place of the p region diffused into the n substrate for the previous device. This improved the injection efficiency of the base-substrate junction and reduced current crowding effects within the base. To aid the future analysis of the MOSBJT, two sets of devices were fabricated. A processing schedule was devised to produce devices with 1000\AA° and $10,000\text{\AA}^\circ$ gate oxides while maintaining identical temperature/time histories (assumes identical diffusion environments).

The silicon wafers were antimony-doped (100) oriented substrate with a $1 \Omega\text{-cm}$ $10 \mu\text{m}$ thick epitaxial layer. The resistivity of the epitaxial layer was measured with four point probe measurements (Table 4.1), which indicated an average resistivity of $\sim 1.0 \Omega\text{-cm}$ (Eqs. 2.4, 2.5).

The fabrication procedure was as follows: The wafers were cleaned (App. A) and a $\sim 5000\text{\AA}^\circ$ oxide (blue) was grown with a 90 minute wet oxidation process (Fig. 1.3). The negative photoresist procedure (App. A) and the isolation mask (Fig. 3.3) was used to define and etch an oxide window. Using the normalized erfc curve (Fig. 3.9), it was established that a 7 hour 1150°C phosphorous predep was appropriate. The wafers were given a HF dip to remove the P_2O_5 glass and negative photoresist was used to etch the n^- diffusion window (Fig. 3.4). A phosphorous predep was performed at 800°C for 15 minutes to provide an

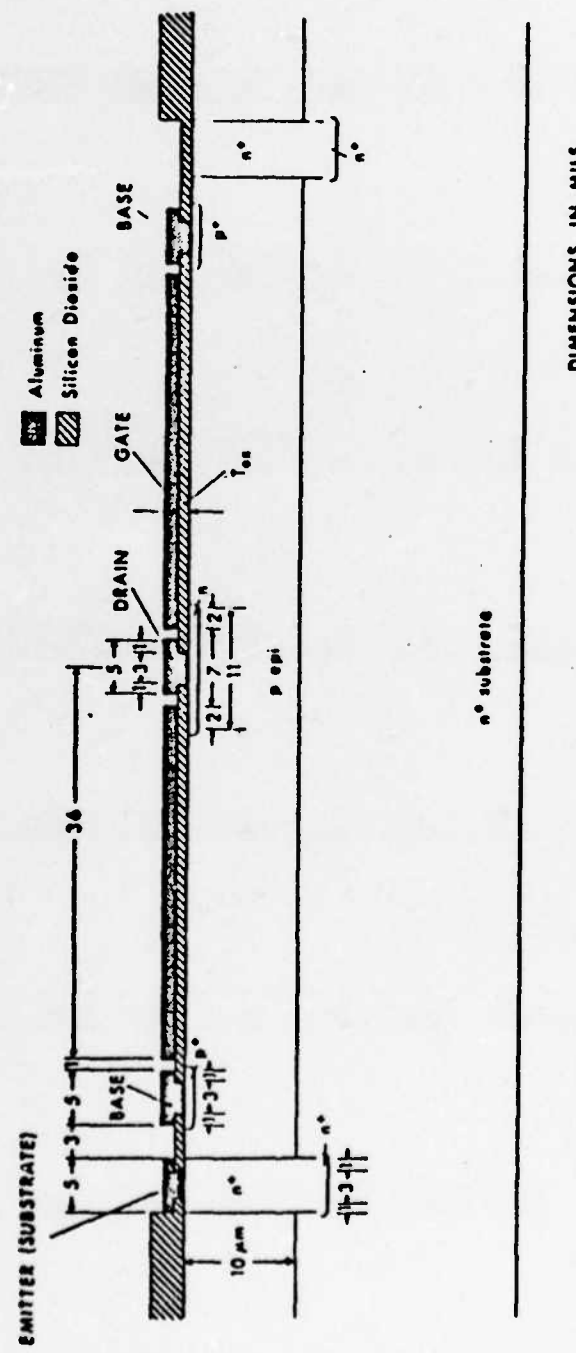


Figure 4.1. Cross sectional view of a MOSBJT with an epitaxial base.

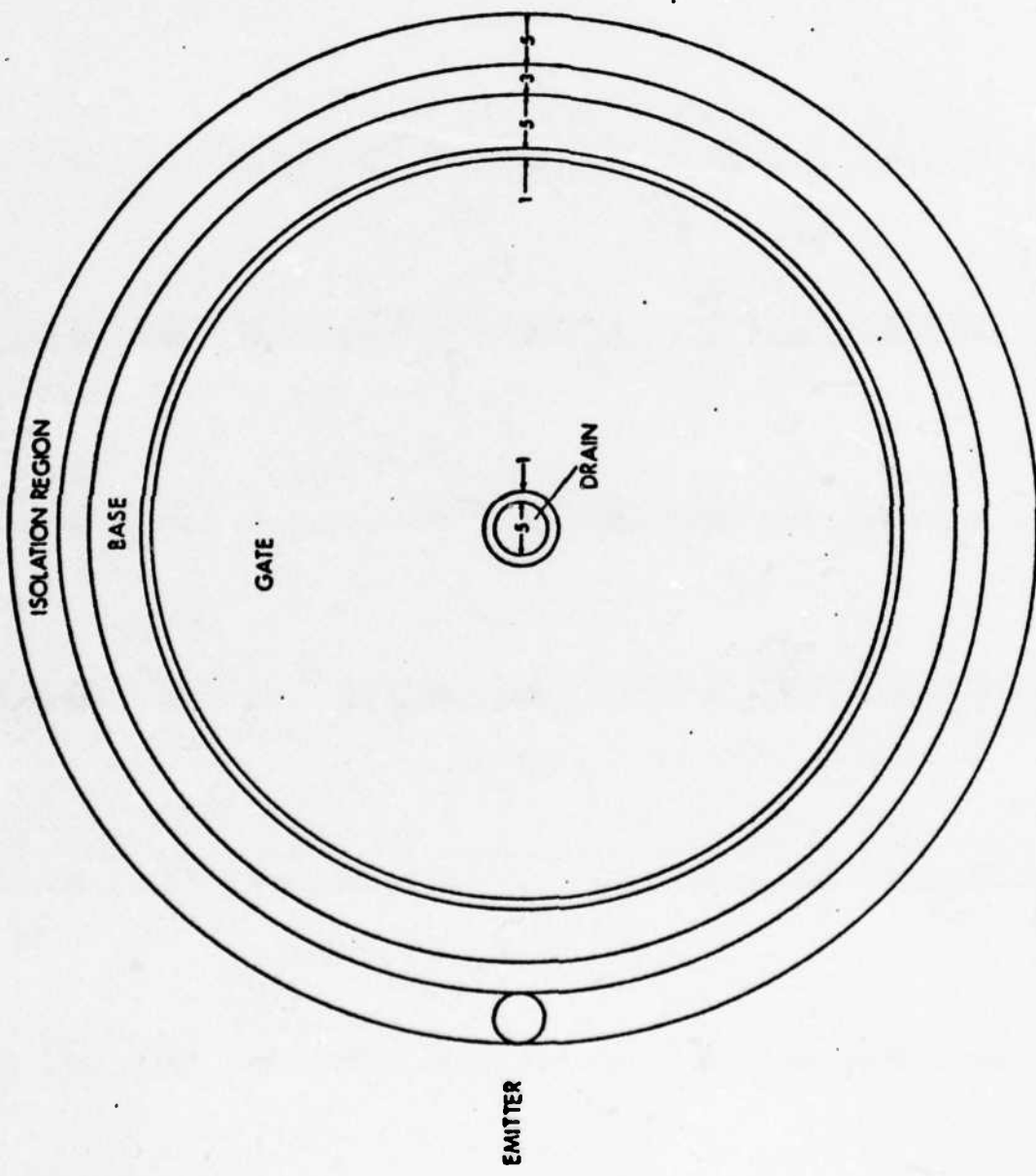


Figure 4.2. Top view of an MOSBJT with an epitaxial base.

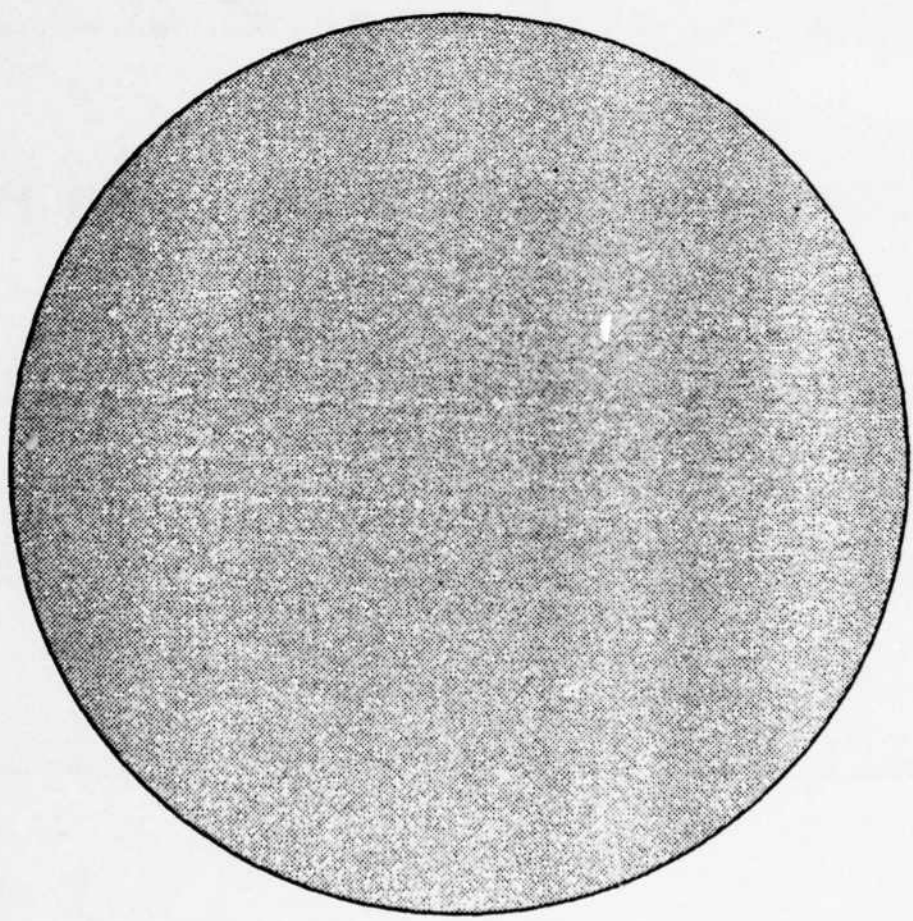


Figure 4.3. Gate oxide regrowth mask.

TABLE 4.1

Four point probe measurements of epitaxial layer

I (mA)	V/I (Ω)	ρ ($\Omega\text{-cm}$)
0.5	240	1.1
0.5	250	1.1
0.5	260	1.2
0.5	210	1.0
1.0	210	1.0
1.0	210	1.0

electrical contact to the inverted MOS channel.

The existing oxide over the gate region was removed using the negative photoresist procedure (App. A) and the gate oxide regrowth mask (Fig. 4.3). For the $10,000\text{\AA}$ gate oxide device a 2 hour 5 minute 1100°C wet oxidation (Fig. 1.3) was completed resulting in a violet oxide $\sim 10,000\text{\AA}$ (App. B). The thin (1000\AA) oxide was grown in two steps in order to expose the device to the same thermal history as the thick ($10,000\text{\AA}$) oxide device and also to consume an equal amount of silicon in its growth, resulting in identical base dimensions: First a wet oxide was grown for 1 hour and 55 minutes at 1150°C and then removed with the negative photoresist procedure (App. A) using the gate oxide regrowth mask (Fig. 4.3); A 10 minute 1150°C wet oxidation process followed resulting in a violet oxide $\sim 1000\text{\AA}$ thick (App. B).

The substrate and drain contact diffusion windows (Fig. 3.5) were opened using negative photoresist and a phosphorous predep was performed at 950°C for 15 minutes to provide the n^+ contact regions. The P_2O_5 glass was removed with a dilute HF etch and a blocking wet oxide was grown over the contact windows (15 minutes, 1000°C). The resulting gate oxides were violet ($\sim 10,000\text{\AA}$) and blue ($\sim 1200\text{\AA}$) (App. B).

Negative photoresist was used with the base contact diffusion mask (Fig. 3.6) to define and etch a window in the SiO_2 for a boron predep, 950°C for 15 minutes and 10 minutes, for the $10,000\text{\AA}$ and 1000\AA oxide devices, respectively. The B_2O_3 glass was removed with a dilute HF etch and a blocking wet oxide was grown for 12 minutes at 1000°C followed by a 45 minute N_2 anneal at 1000°C to reduce the surface state

concentration [2]. The results were violet ($\sim 10,000\text{\AA}$) and blue ($\sim 1200\text{\AA}$ App. B) gate oxides. The metallization contact window mask (Fig. 3.7) was used to define and etch windows in the oxide and aluminum was evaporated at 8×10^{-7} torr. The metallization was defined with positive photoresist (App. A) and the metallization mask (Fig. 3.8).

This MOSBJT fabricated with an epitaxial base was characterized using a Tektronix 576 curve tracer (Fig. 4.4). The effect of gate voltage on the BJT characteristics of the 1200\AA and $10,000\text{\AA}$ devices are displayed in Figs. 4.5 and 4.7, respectively. Compared to the previous MOSBJT devices (Sec. 2.3) the maximum gain increased to ~ 1 , probably the result of the favorable injection efficiency of the base (epitaxial layer)/emitter (substrate) junction. A factor that may be degrading the base/emitter injection efficiency is the interdiffusion of the antimony from the n^+ substrate into the base during the high temperature processes forming a graded junction. The reverse BJT characteristics illustrated in Figs. 4.6 and 4.8 reveal a gain of ~ 50 and 20. This is lower than the MOSBJT fabricated with a diffused base and could result from the reduction of the base minority carrier diffusion length due to recombination lifetime degradation caused by defects such as stacking faults or dislocations in the epitaxial layer.

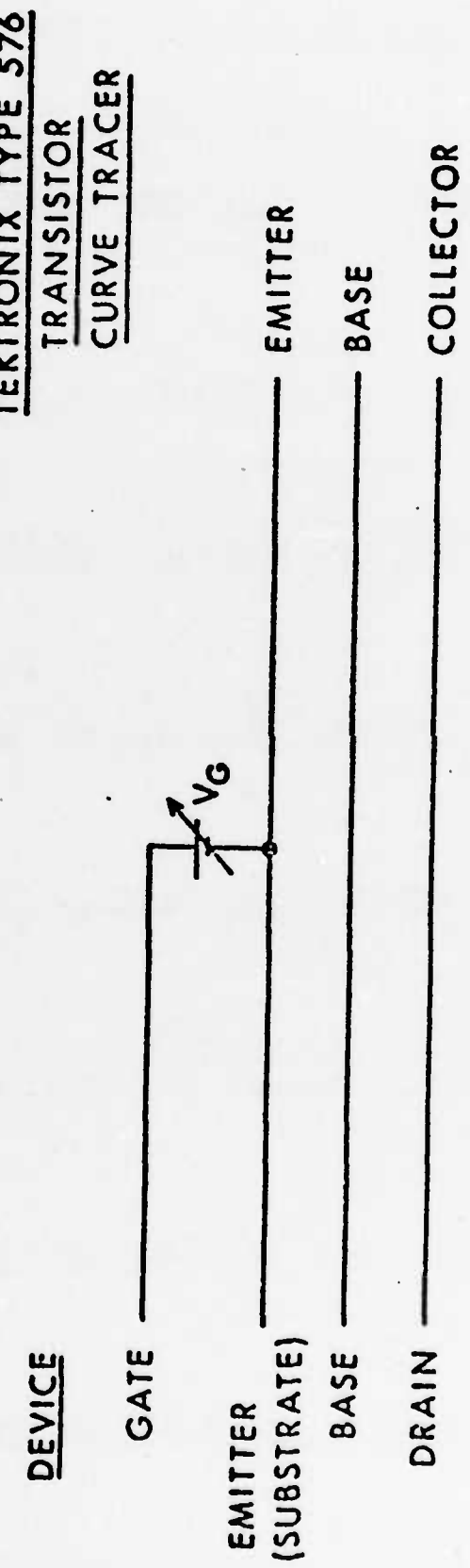


Figure 4.4. Test circuit used for the MOSBJT having an epitaxial base.

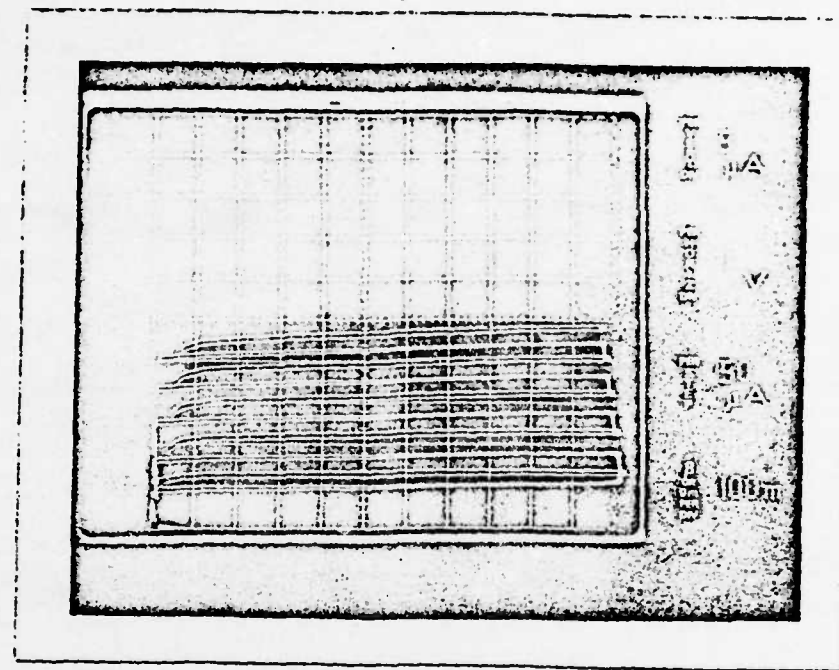


Fig. 4.5a. $V_G = -5V$.

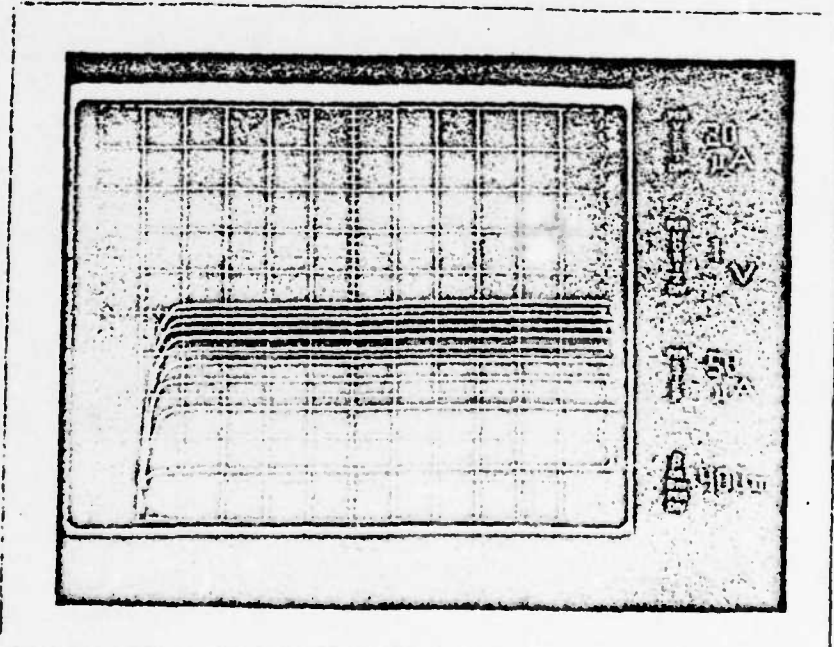


Fig. 4.5b. $V_G = 0V$.

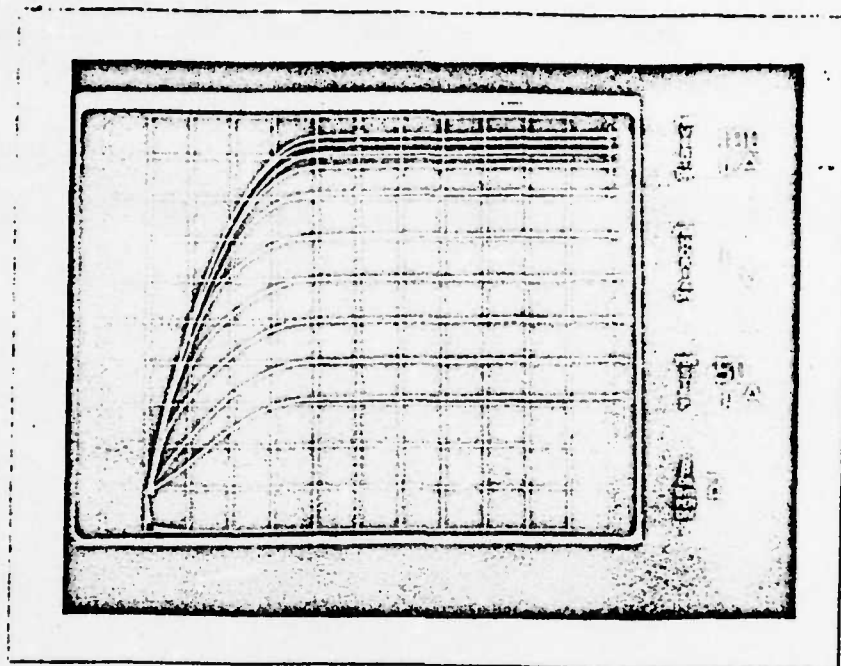


Fig. 4.5c. $V_G = 5V.$

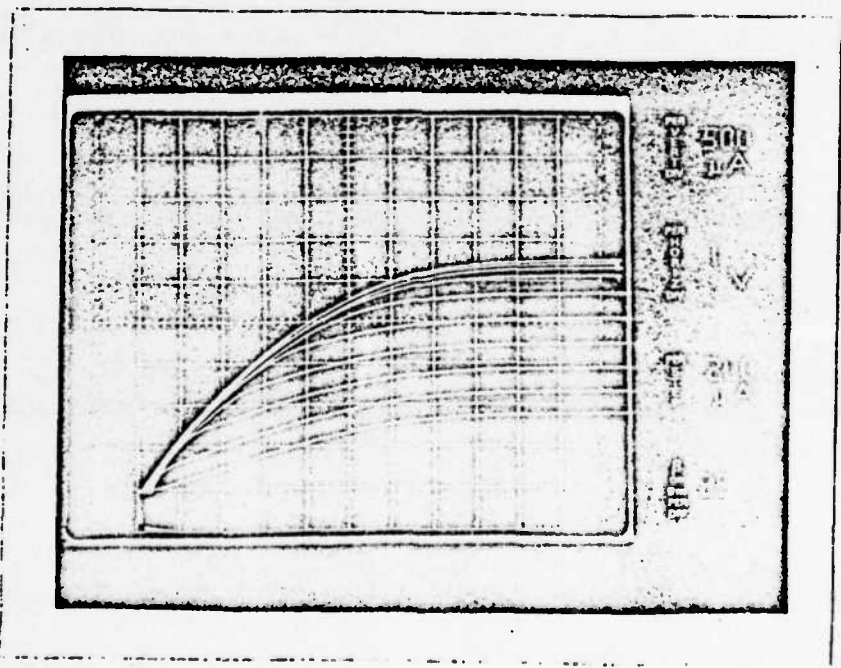


Fig. 4.5d. $V_G = 10V.$

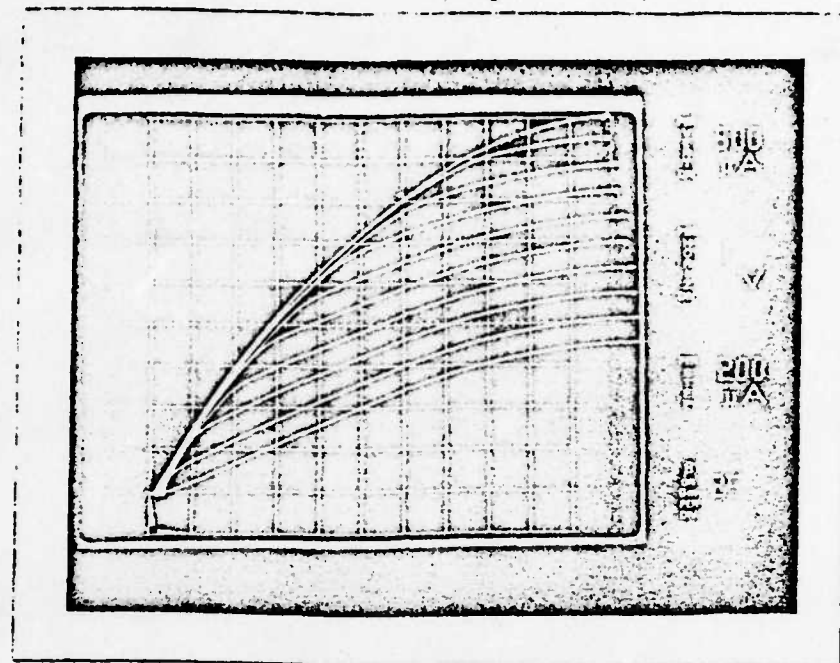


Fig. 4.5e. $V_G = 15V$.

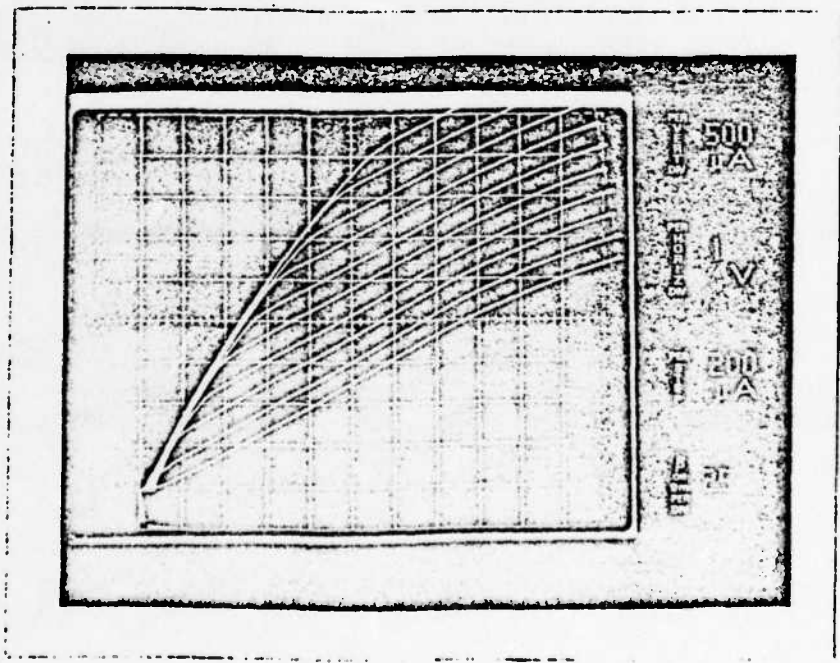


Fig. 4.5f. $V_G = 20V$.

Figure 4.5. MOSBJT (epitaxial base) BJT characteristics as a function of gate voltage. Gate oxide is 1200Å.

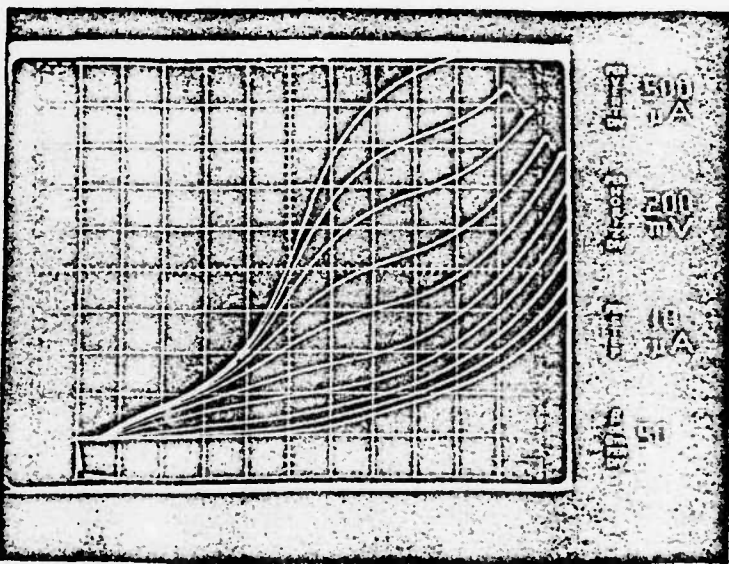


Figure 4.6. MOSBJT (epitaxial base) reverse BJT characteristics. Gate oxide is 1200\AA .

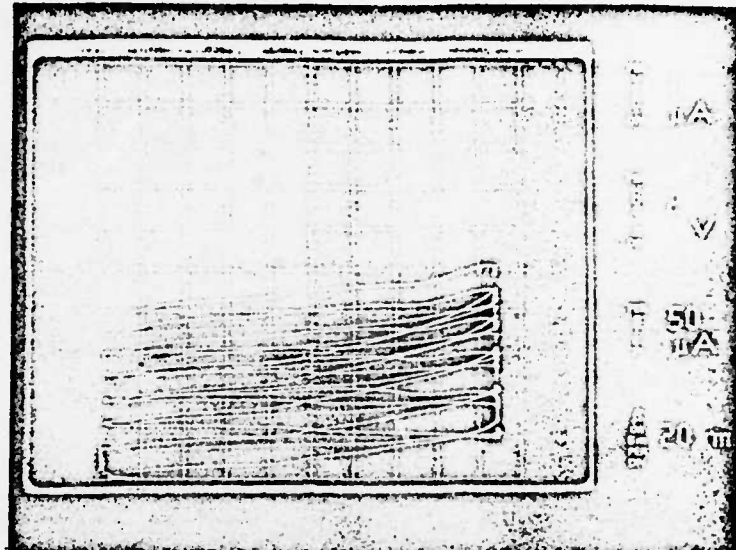


Fig. 4.7a. $V_G = 0V$.

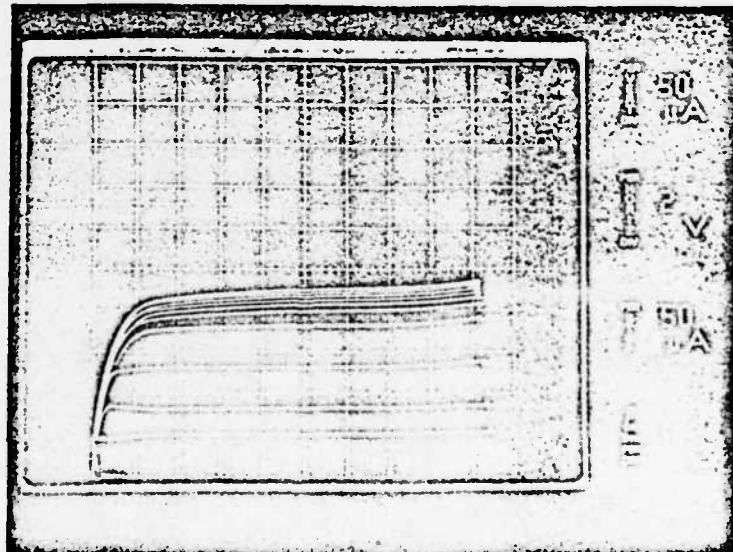


Fig. 4.7b. $V_G = 10V$.

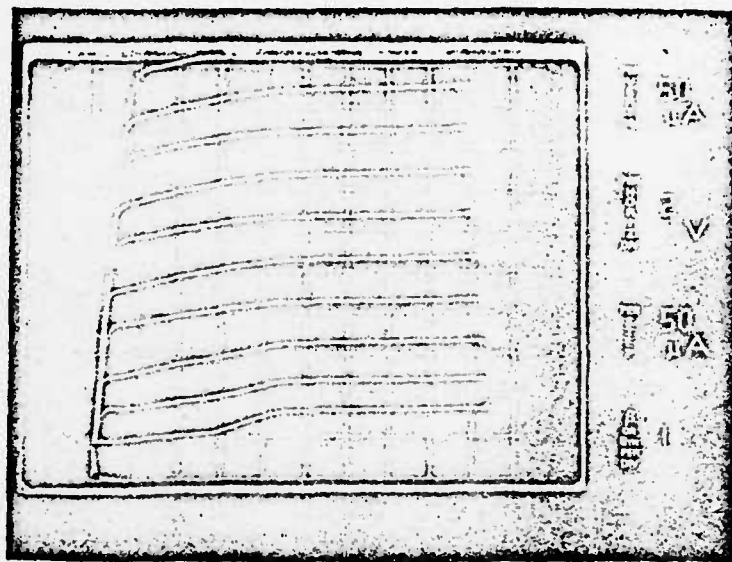


Fig. 4.7c. $V_G = 30V.$

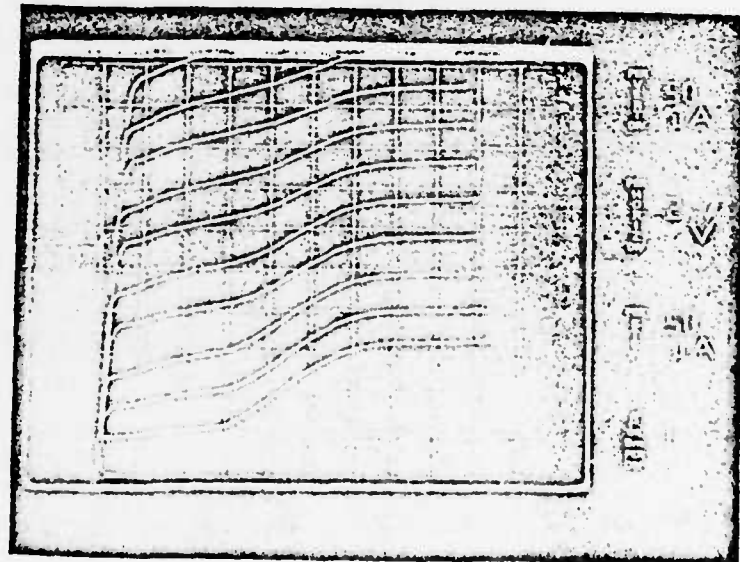


Fig. 4.7d. $V_G = 40V.$

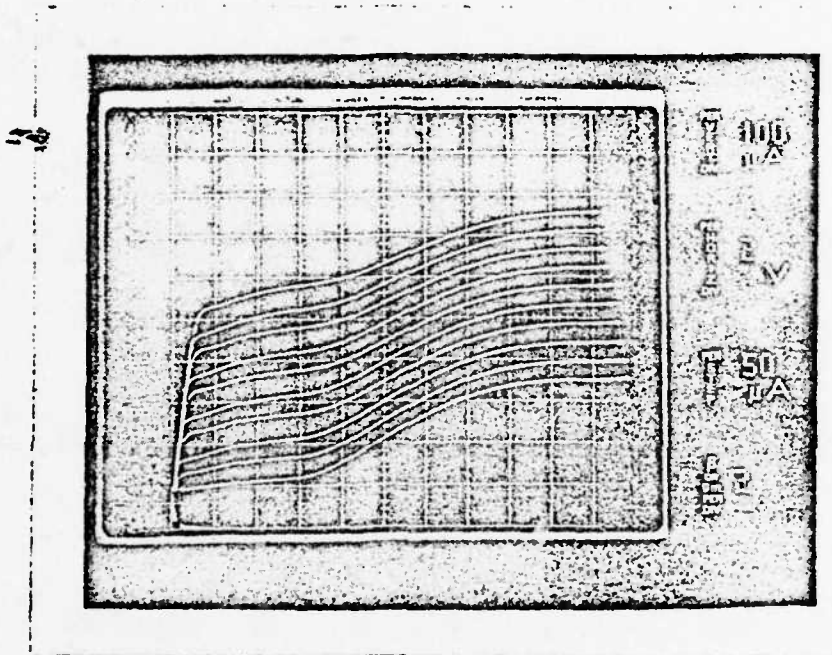


Fig. 4.7e. $V_G = 50V$.

Figure 4.7. MOSBJT (epitaxial base) BJT characteristics
as a function of gate voltage. Gate oxide
is $10,000\text{\AA}$:

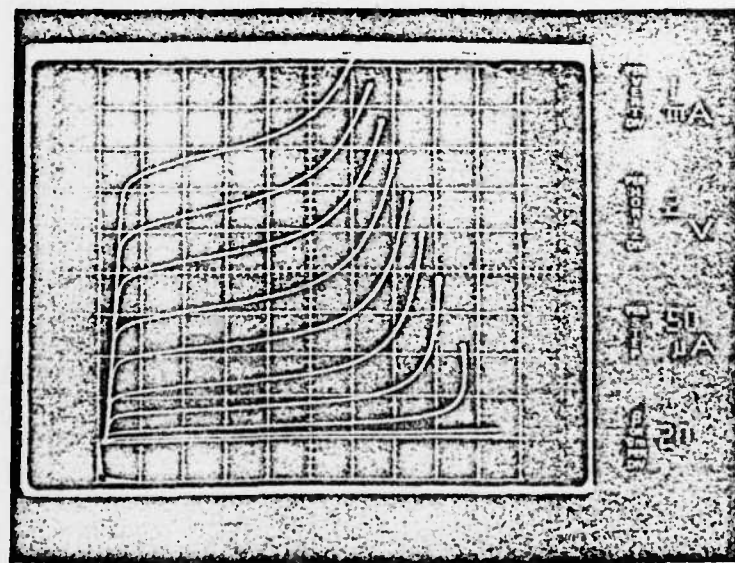


Figure 4.8. MOSBJT (epitaxial base) reverse BJT characteristics. Gate oxide is 10,000 \AA .

2.5 MOSBJT Having an Epitaxial Base and a Mesa Etched Isolation Region

One cause of the low gain in the previous MOSBJTs is probably the diffusion of antimony from the substrate into the base epitaxial layer degrading the injection efficiency of the base-substrate junction. To reduce the Sb diffusion and thereby increase the gain, devices were fabricated with an etched isolation region (Fig. 5.2), eliminating the long isolation diffusion and relative high temperature processing.

The (100) oriented silicon wafers consisted of a 10 μ m, 1 Ω -cm resistivity, p-type epitaxial layer grown on a n⁺ antimony-doped substrate. To etch the 10 μ m deep isolation ring the negative photoresist procedure (App. A) was followed except that CP-4 was used instead of buffered HF. CP-4's chemical activity varies with temperature and from batch to batch and required testing to determine whether the photoresist could withstand the etchant and to characterize the etch rate. To decrease the activity of the CP-4, it was diluted 10:1::CP-4:DI. A test silicon wafer was etched and measurements with a micrometer established that a 3 minute etch was sufficient to remove 10 μ m of silicon. Before the wafers were etched, negative photoresist was used to protect the back of the wafer from the etchant, reducing the heating and undesirable increase in chemical activity of the CP-4. Device isolation was verified when I-V characteristics between the central regions of two isolation rings were "back to back" diode characteristics. These characteristics result from the p-epitaxial layer/n⁺ substrate/p-epitaxial layer structure that occurs when the isolation ring etches through the epitaxial layer.

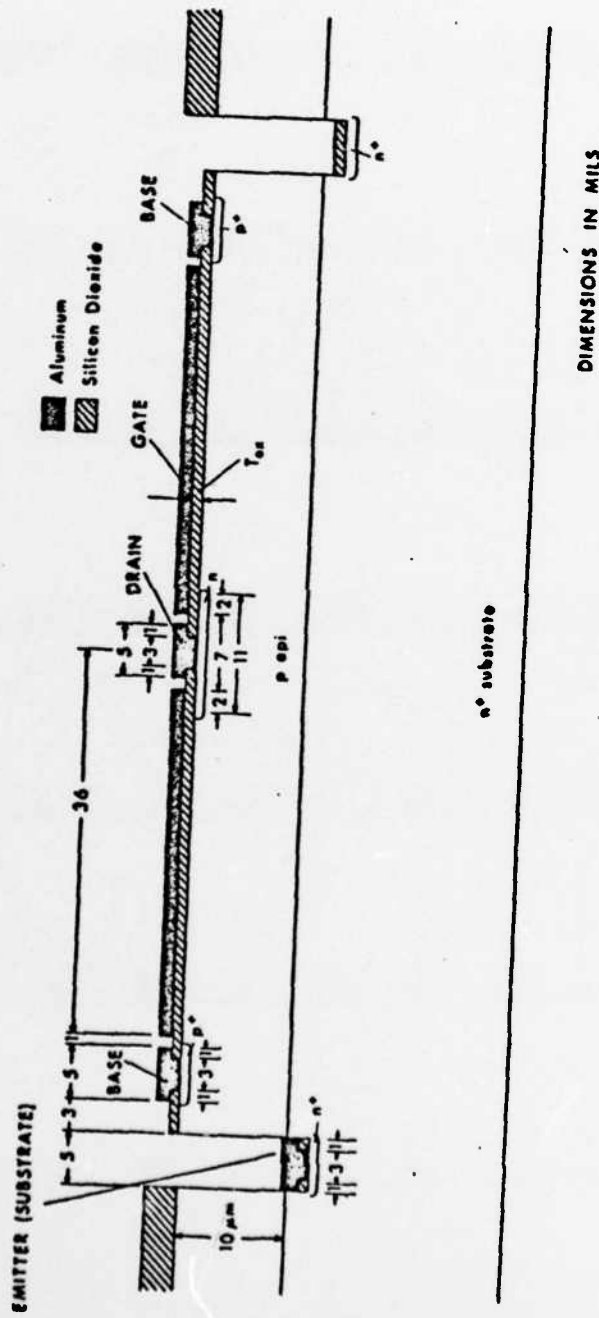


Figure 5.1. Cross-sectional view of MOSBJT with an etched isolation ring.

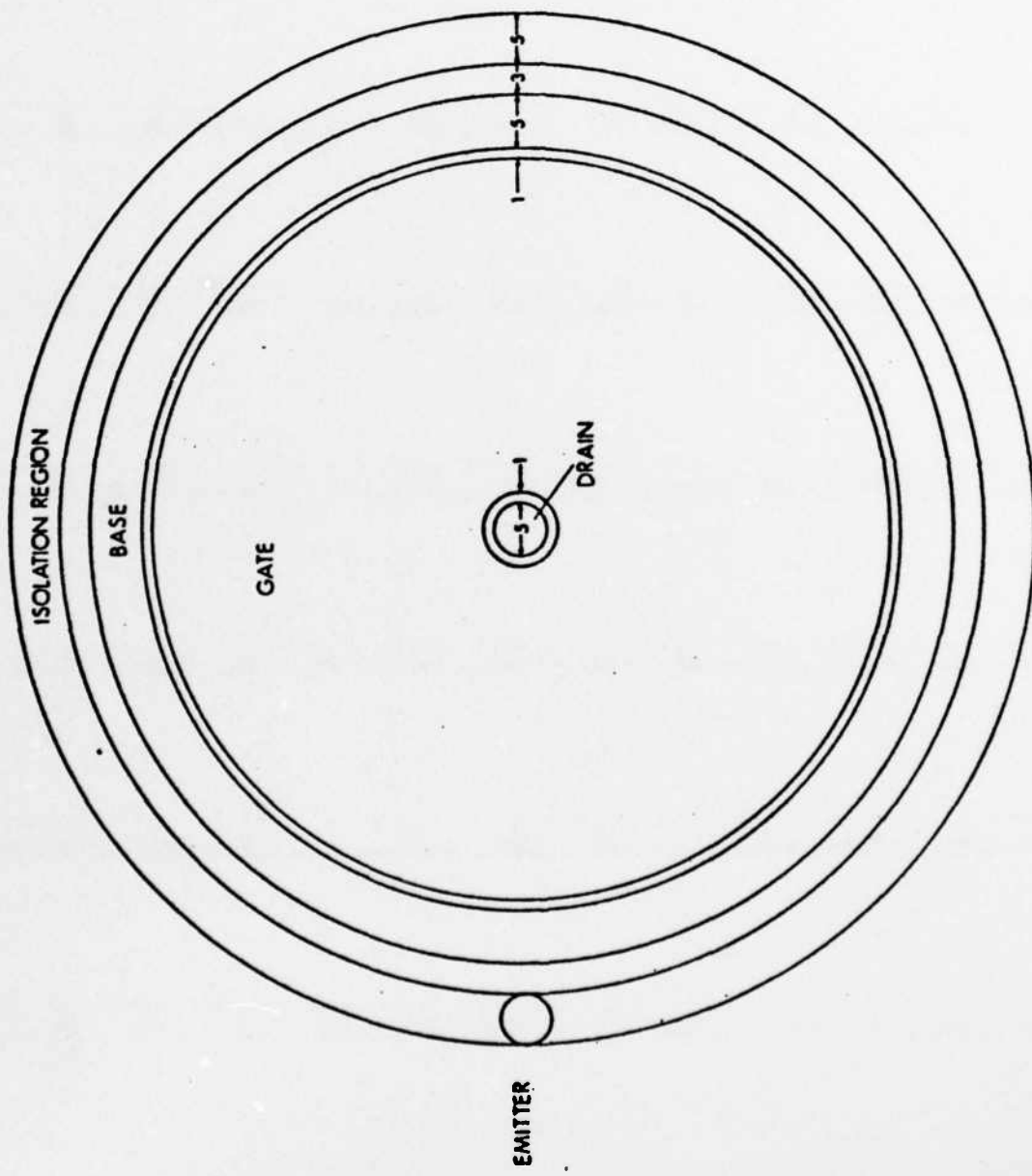


Figure 5.2. Top view of MOSBJT with an etched isolation ring.

The remaining fabrication of the 1000\AA gate oxide devices proceeded as follows. The wafers were cleaned (App. A) and a 90 minute 1000C wet oxide grown. The negative photoresist procedure was used with the n^- drain diffusion mask (Fig. 3.4) and isolation mask (Fig. 3.3) to define and etch windows in the oxide. A phosphorous predep was performed at 950C for 15 minutes. The P_2O_5 glass was removed with a dilute HF and a 15 minute 1000C wet blocking oxide was grown. The base contact diffusion mask (Fig. 3.7) was used in the negative photoresist procedure (App. A) to open windows in the oxide for a 15 minute 950C boron predep. The existing oxide over the gate region was removed (gate oxide regrowth mask--Fig. 4.3, negative photoresist procedure). The gate oxide was grown dry at 1000C for 100 minutes and nitrogen annealed [2]. The resulting gate oxide color was royal blue corresponding to 1200\AA (App. B). Negative photoresist was used to define and etch the drain, base, and substrate metallization contact windows (Fig. 3.8). Aluminum was evaporated at 8×10^{-7} torr and metal pads defined (positive photoresist, App. A, metallization mask, Fig. 3.8).

Fabrication procedure for the $10,000\text{\AA}$ MOSBJT was as follows. Identical wafers were used. The isolation ring was etched in the same manner as the previous 1200\AA oxide devices. A blocking oxide (wet, 90 minute, 1000C) was grown resulting in a royal blue color corresponding to $\sim 4900\text{\AA}$ (App. B). The n^- drain diffusion mask (Fig. 3.4) and the isolation mask (Fig. 3.3) were used to etch windows in the oxide for a 15 minute 800C phosphorous predep. The existing oxide over the gate was removed (negative photoresist, App. A, gate oxide regrowth mask,

Fig. 4.3) and the gate oxide was grown wet for 2 hours and 5 minutes at 1100°C ($\sim 10,000\text{\AA}$, Fig. 1.3). The substrate and drain contact diffusion windows (Fig. 3.5) were defined and etched (negative photoresist, App. A) and a 950°C, 15 minute phosphorous predep was performed to provide the n^+ substrate and drain contact regions. The P_2O_5 glass was removed with a dilute HF etch and a wet oxide was grown for 15 minutes at 1000°C. To ensure that the aluminum forms a good ohmic contact with the p epitaxial layer, the base contact window (Fig. 6) was defined using negative photoresist, etched, and a 15 minute, 950°C boron predep performed. Dilute HF removed the B_2O_3 and a wet blocking oxide was grown for 15 minutes at 1000°C. The negative photoresist procedure was used to define and etch the metallization contact windows (Fig. 3.7) and aluminum was evaporated at 8×10^{-7} torr. The metallization was defined with positive photoresist and the metallization mask (Fig. 3.8).

The MOSBJT fabricated with an epitaxial base and mesa etched isolation region was characterized with a Tektronix 576 curve tracer in the circuit shown in Fig. 5.3. The effect gate voltage has on the BJT characteristics is revealed in Figs. 5.4 and 5.6 for the 1200\AA and $10,000\text{\AA}$ devices, respectively. The maximum gain was ~ 3 for the 1200\AA device and ~ 2 for the $10,000\text{\AA}$ device. The gain of these devices are slightly larger than the MOSBJT with a diffused isolation region probably the result of the elimination of the isolation diffusion. This reduces the degree of interdiffusion of antimony into the epitaxial layer and therefore probably increases the injection efficiency of the

emitter/base junction. The relatively slight increase in gain resulting from the reduction of a significant amount of high temperature processing implies that the interdiffusion of antimony into the base may not be the major cause of the low gain of the MOSBJT.

The reverse BJT characteristics of the device was observed by using the drain as the emitter and the substrate as the collector. The reverse characteristics of the 1200A° and the $10,000\text{A}^{\circ}$ devices shown in Figs. 5.5 and 5.6 reveal a gain of 50 and 25, respectively. The consistent low reverse gain of the MOSBJT devices with an epitaxial base layer indicates that the epitaxial layer may be the major cause of the low gain. As mentioned previously this may be caused by a short minority carrier lifetime in the base epitaxial layer due to recombination of defects. Also lattice strain at the forward biased epitaxial layer (base)/substrate (emitter) interface may be causing substantial amount of recombination which would result in a large increase in base current and therefore a significant reduction in gain.

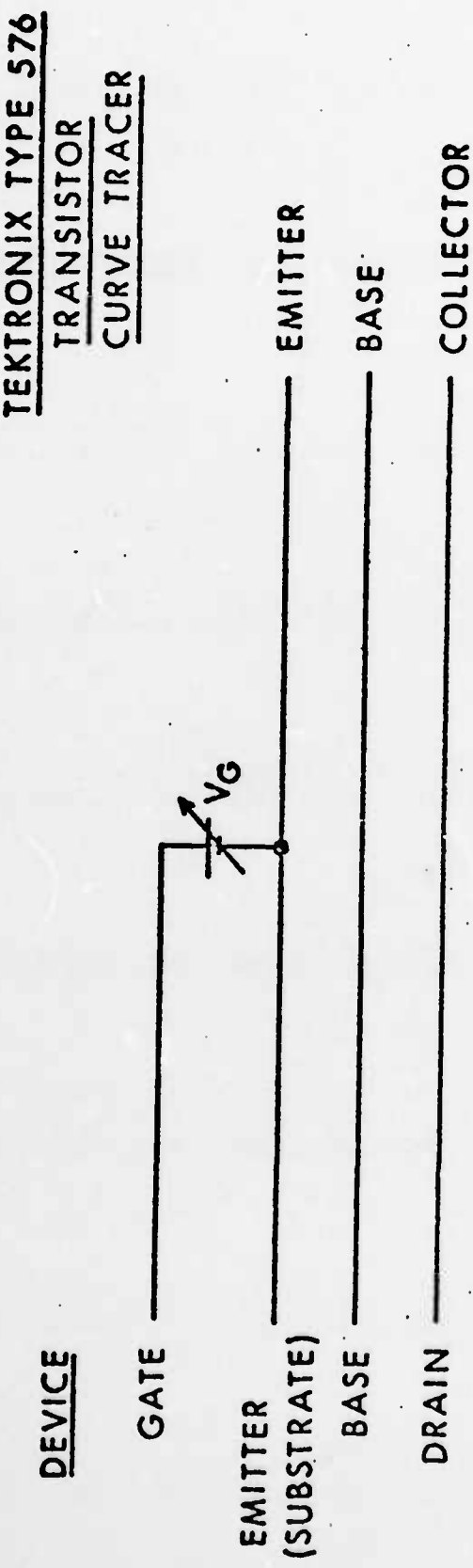


Figure 5.3. Test circuit configuration for the MOSBJT having an epitaxial base and a mesa etched isolation region.

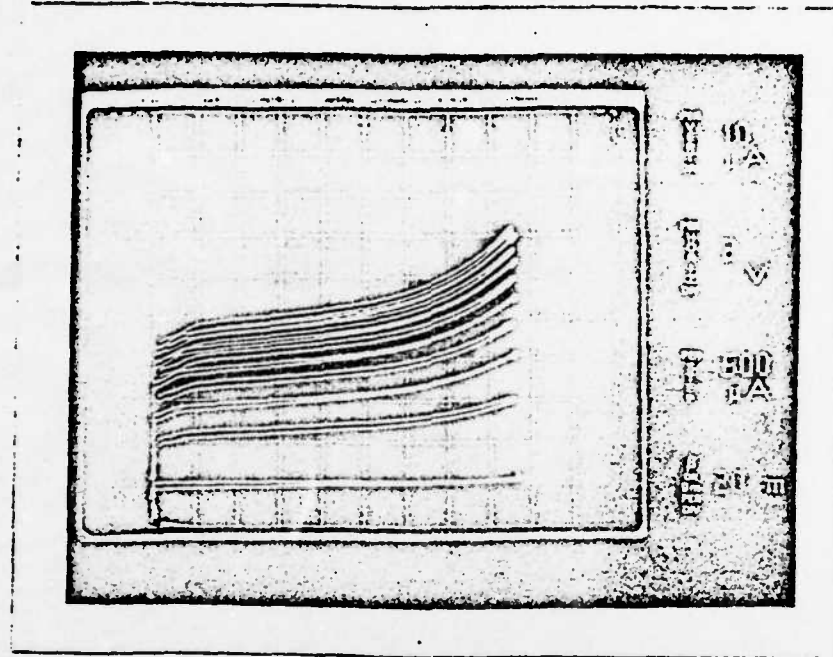


Fig. 5.4a.. $V_G = 0V.$

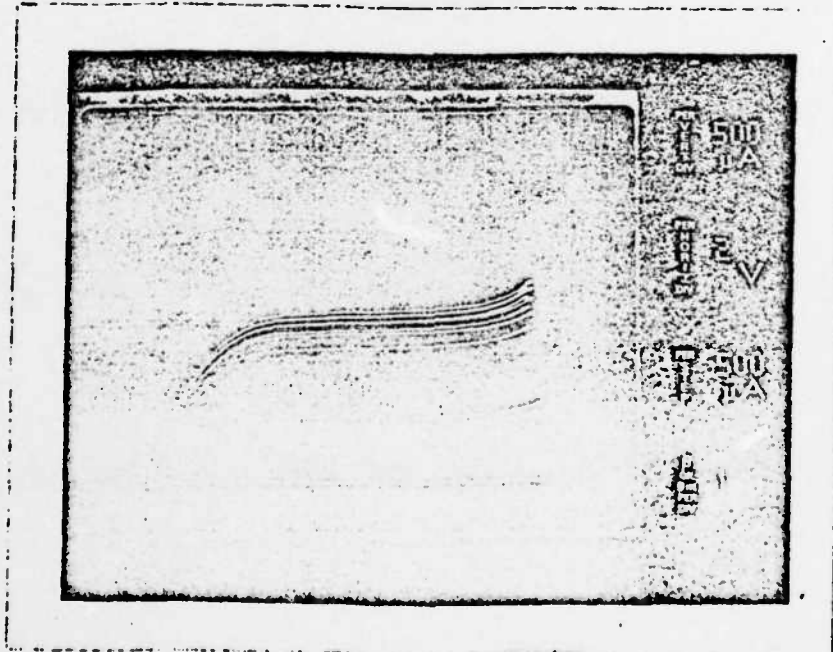


Fig. 5.4b. $V_G = 10V.$

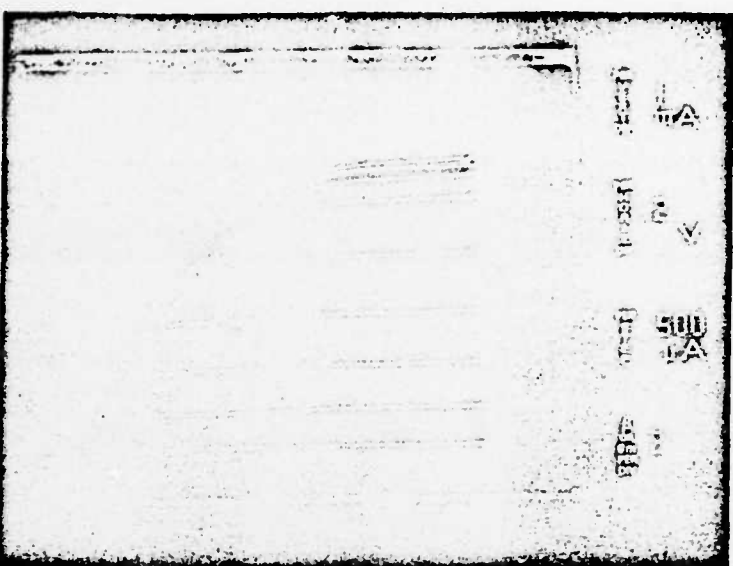


Fig. 5.4c. $V_G = 20V$.

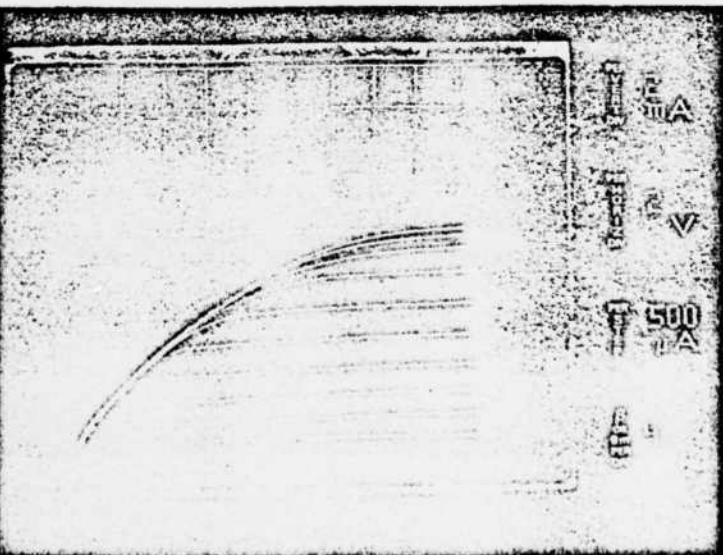


Fig. 5.4d. $V_G = 25V$.

Figure 5.4. MOSBJT (epitaxial base, mesa etched isolation) BJT characteristics as a function of gate voltage.
Gate oxide is 1200Å .

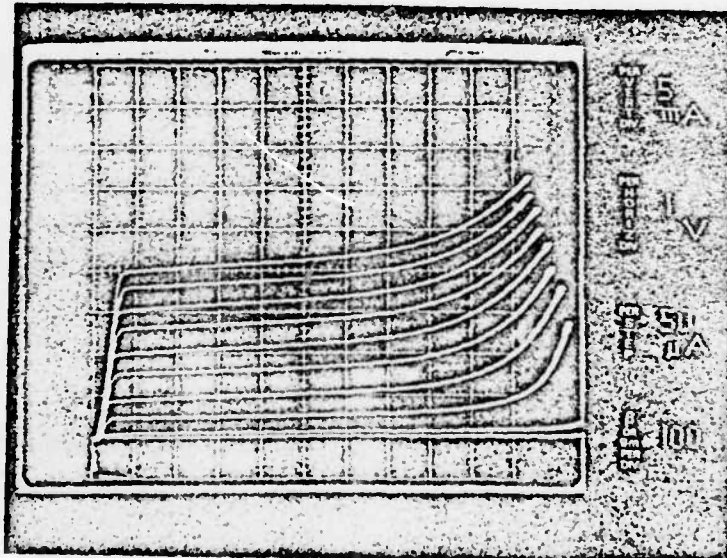


Figure. 5.5. MOSBJT (epitaxial base, mesa etched isolation)
reverse BJT characteristics as a function of
gate voltage. Gate oxide is 1200\AA .

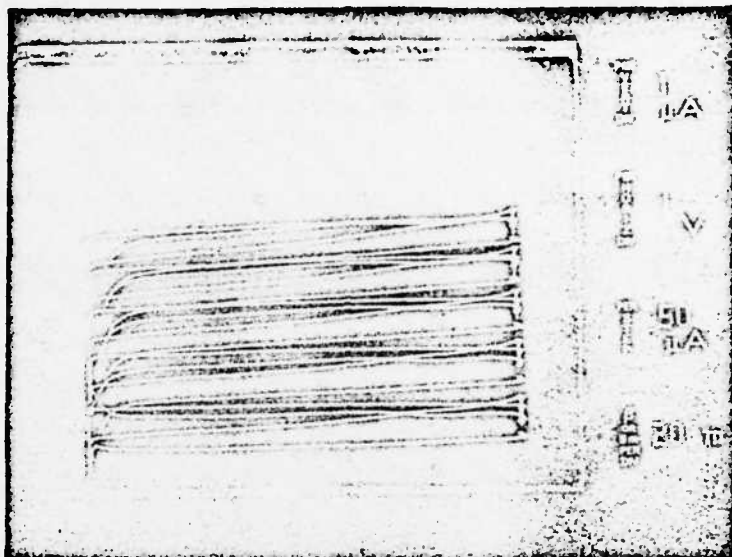


Fig. 5.6a. V_G = negative.

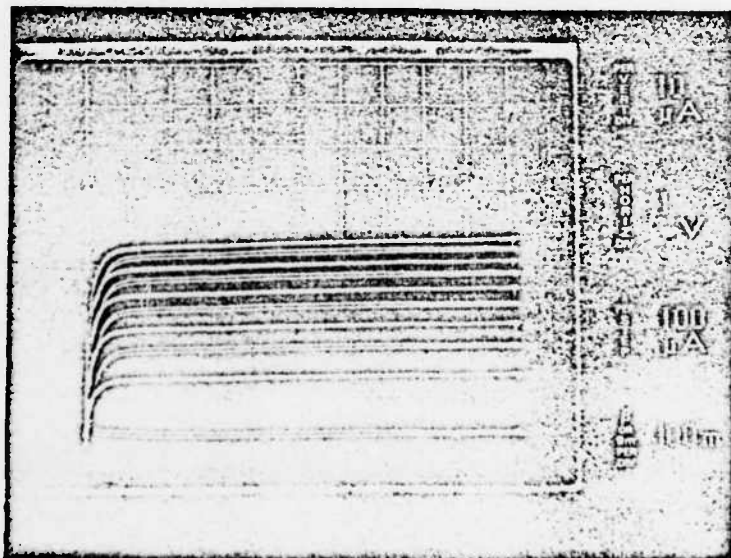


Fig. 5.6b. V_G = 10V.

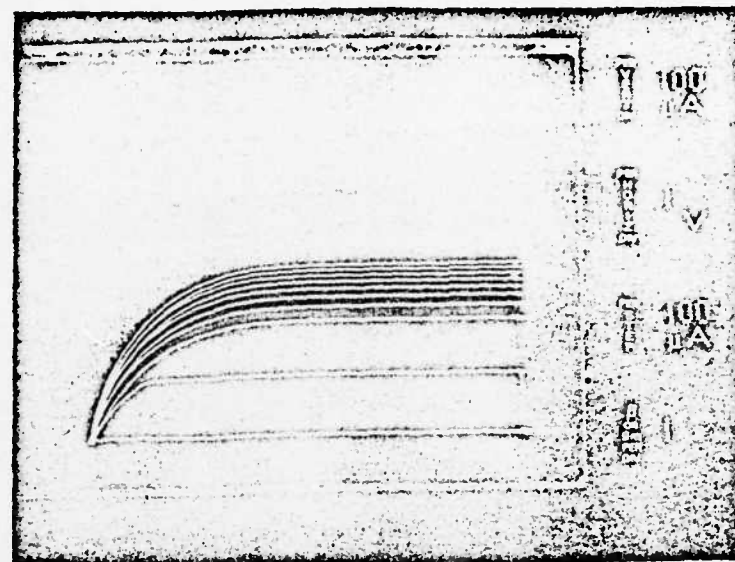


Fig. 5.6c. $V_G = 30V.$

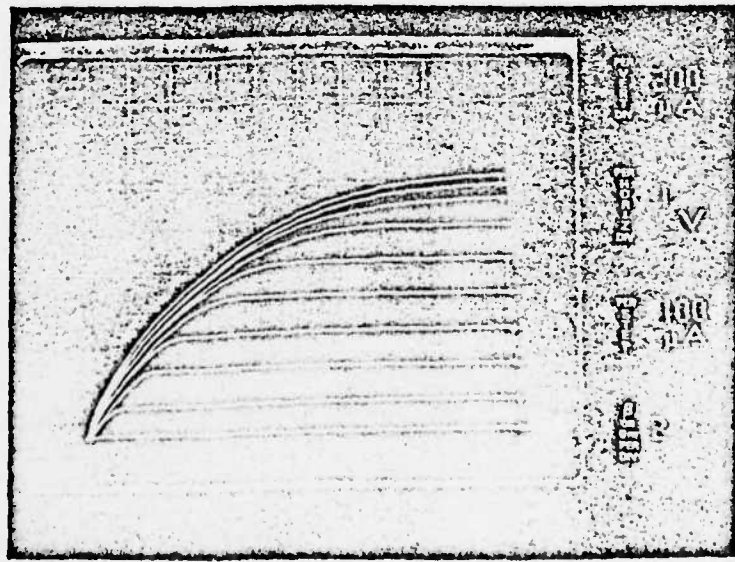


Fig. 5.6d. $V_G = 50V.$

Figure 5.6. MOSBJT (epitaxial base, mesa etched isolation)
BJT characteristics as a function of gate
voltage. Gate oxide is $\sim 10,000\text{Å}^{\circ}$.

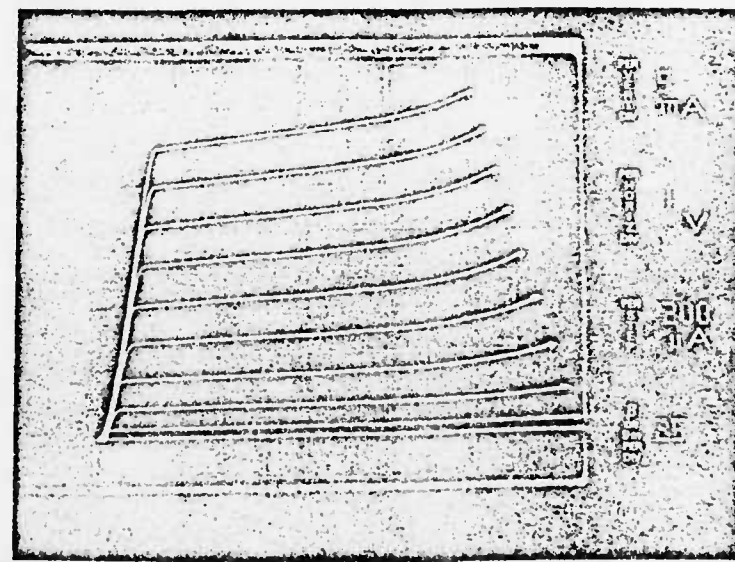


Figure 5.7. MOSBJT (epitaxial base, mesa etched isolation) reverse BJT characteristics as a function of gate voltage. Gate oxide is $\sim 10,000\text{\AA}$.

FID-A132 332

FABRICATION OF A SILICON MOSFET DEVICE WITH BIPOLAR
TRANSISTOR SOURCE(U) HAWAII UNIV AT MANOA HONOLULU DEPT
OF ELECTRICAL ENGINEERING D N OKADA JUL 80

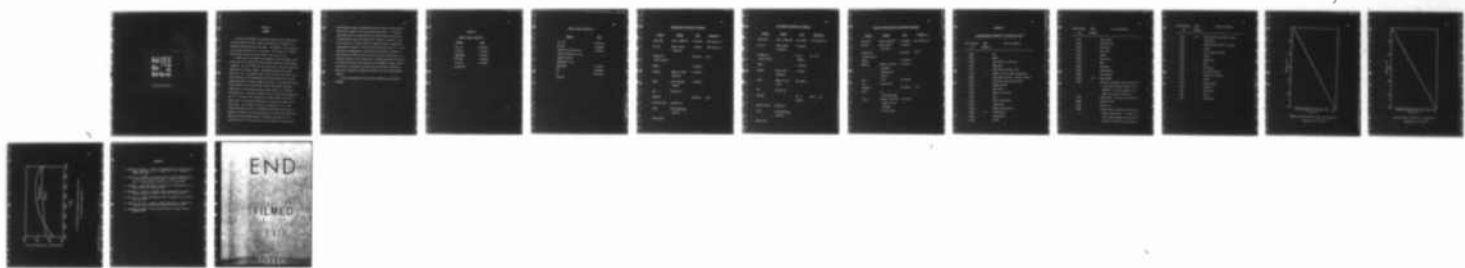
2/2

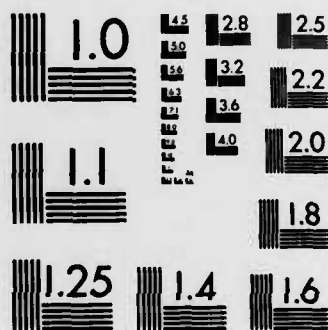
UNCLASSIFIED

N00014-76-C-1081

F/G 9/1

NL





MICROCOPY RESOLUTION TEST CHART
NATIONAL BUREAU OF STANDARDS-1963-A

CHAPTER 3

SUMMARY

To verify that MOSFETs of acceptable quality could be fabricated at the University of Hawaii Physical Electronics Lab a MOSFET of a straight forward design was fabricated. The MOSFET was then constructed in a p region diffused into a n substrate. This resulted in a MOSFET with a bipolar source which had a bipolar gain (β) of ~ 0.3 .

A novel device (the MOSBJT) was designed to provide bipolar transistor gain and to confine electron injection into the inverted MOSFET n-channel. The first MOSFET was fabricated with a diffused p-type base region and n⁺ isolation region. The maximum bipolar gain of this device was ~ 0.8 . A probable cause of the low gain was the poor injection efficiency of the base-emitter junction resulting from a linear graded junction and a heavily doped base region. To increase the injection efficiency of the emitter-base junction the diffused base was replaced by a 1 Ω-cm p-type epitaxial layer grown on a n⁺ antimony doped substrate. The bipolar transistor gain of these devices increased to ~ 1.0 . To reduce the interdiffusion of the antimony into the epitaxial layer the isolation diffusion was replaced by an etched isolation region. This resulted in the gain increasing to ~ 2.0 . The slight improvement in gain of the MOSBJT implies that the low gain is probably not totally due to the degradation of the injection efficiency resulting from the interdiffusion of antimony into the base. The reverse BJT gain (in which the drain is the emitter and the substrate,

the collector) showed a significant decrease in gain for the epitaxial base devices compared with the diffused base devices. This implied that defects such as stacking faults and dislocations may be present in the epitaxial layer and reducing the lifetime in the base. Since the Sb substrate is heavily doped, a substantial defect concentration (recombination centers) in the emitter-base depletion layer is probable. Substantial recombination in the forward biased emitter (substrate)-base (epitaxial layer) junction and within the base could cause a significant increase in base current with a related suppression of the gain. The final device goals were achieved with the MOSBJT in which a MOSFET and BJT were successfully integrated while maintaining satisfactory gain with a substantial controlled injection into the inverted MOSFET channel.

At this time experiments for which the MOSBJT was conceived are underway.

APPENDIX A

WAFER CLEANING PROCEDURE 1

<u>Process</u>	<u>Time</u>
10:1 HF	10 seconds
DI rinse	2 minutes
H_2SO_4/H_2O_2	5 minutes
DI rinse	5 minutes
DI rinse	5 minutes
N_2 Blow Dry	

WAFER CLEANING PROCEDURE 2

<u>Process</u>	<u>Time</u>
10:1 HF	10 seconds
DI rinse	2 minutes
Ultrasonic agitation and gentle scrubbing in a hot Joy/DI solution	2 minutes
Thorough DI rinse	
H ₂ SO ₄ /H ₂ O ₂	5 minutes
DI	5 minutes
DI	10 minutes
Spin dry	

KMER NEGATIVE PHOTORESIST PROCEDURE

<u>Process</u>	<u>Method</u>	<u>Time</u>	<u>Temperature</u>
Coat wafer	Spin at 4000 RPM	15 seconds	Room temperature
Air dry	Under laminar flow hood	3 minutes	Room temperature
Prebake the resist coating		20 minutes	80°C
Expose		6 seconds	
Develop	Immerse in KMER developer	3 minutes	
Rinse	With isopropyl alcohol	3 minutes	
Dry	N ₂ blow dry		
Postbake		15 minutes	100°C
Etch the oxide	Buffered HF		
Strip	Using H ₂ SO ₄ /H ₂ O ₂ solution		
Clean wafers			

KTI NEGATIVE PHOTORESIST PROCEDURE

<u>Process</u>	<u>Method</u>	<u>Time</u>	<u>Temperature</u>
Coat wafer	Spin at 4000 RPM	15 seconds	Room temperature
Air dry	Under laminar flow hood	3 minutes	
Prebake the resist coating		25 ± 5 minutes	90 ± 5°C
Expose		6 seconds	
Develop	Soak in KTI developer	1 minute	
Rinse	Immerse in KTI rinse	30 seconds	
Dry	N ₂ blow dry		
Postbake		25 ± 5 minutes	140°C ± 5°C
Etch the oxide	Buffered HF		
Strip	Using H ₂ SO ₄ /H ₂ O ₂ solution		
Clean wafer			

SHIPLEY AZ-1360J POSITIVE PHOTORESIST PROCEDURE

<u>Process</u>	<u>Method</u>	<u>Time</u>	<u>Temperature</u>
Coat wafer	Spin at 4000 RPM	15 seconds	Room temperature
Air dry	Under laminar flow hood	3 minutes	
Prebake the resist coating		15 minutes	100°C
Expose		6 seconds	
Develop	Immerse in AZ-606 developer dilluted 10:1 with DI	25 seconds	
Rinse	In DI	10 seconds	
Dry	N ₂ blow dry		
Postbake		15 minutes	95°C
Etch	In 20:1::H ₃ PO ₄ :HNO ₃		
Strip	Immerse in Shipley remover--1112A dilluted 2:1::DI:1112A	30 seconds	

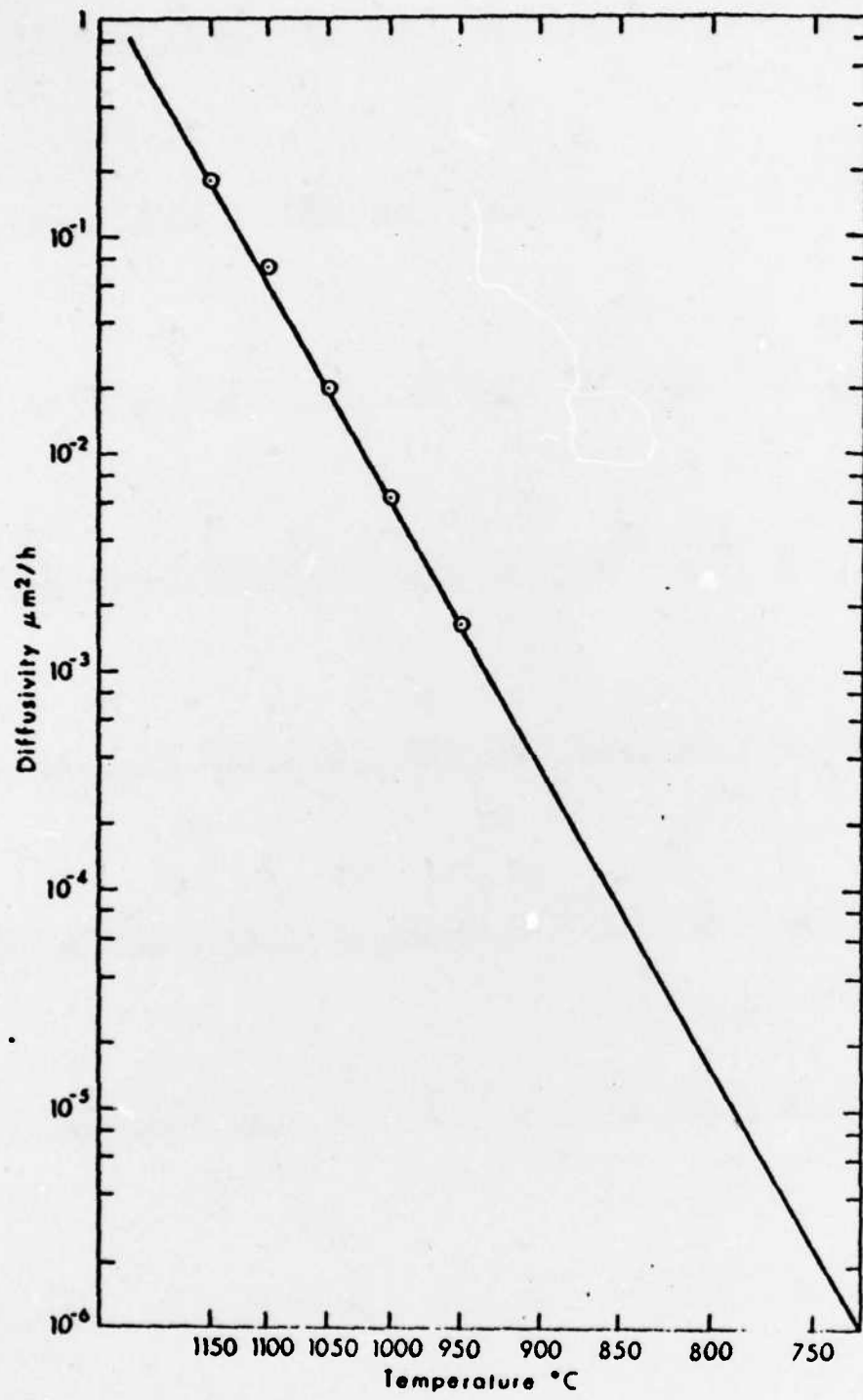
APPENDIX B

SILICON DIOXIDE THICKNESS VS. INTERFERENCE COLOR⁷

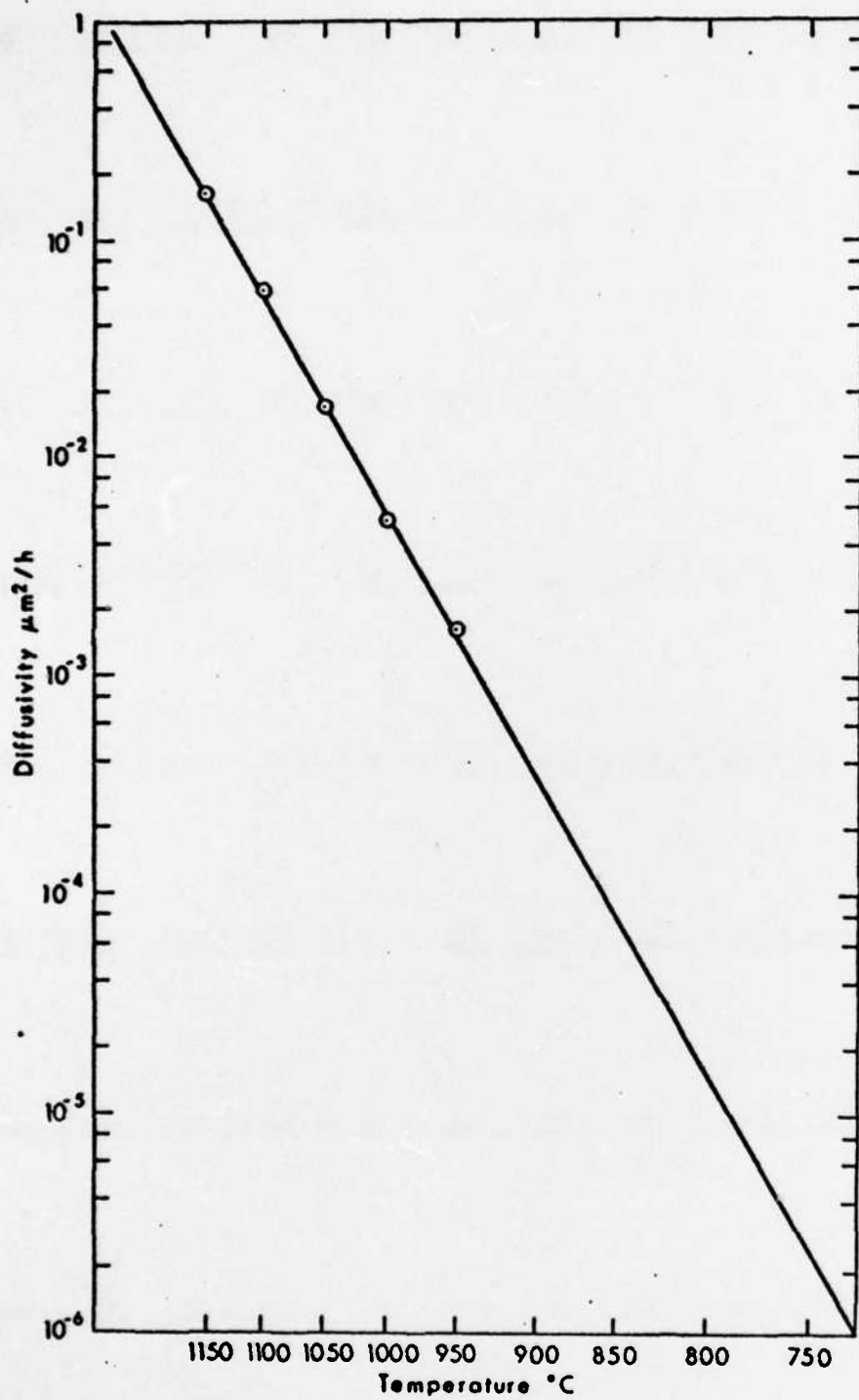
Film Thickness (μ)	Order (5460 Å)	Color and Comments
0.05 ₀		Tan
0.07 ₅		Brown
0.10 ₀		Dark violet to red-violet
0.12 ₅		Royal blue
0.15 ₀		Light blue to metallic blue
0.17 ₅	I	Metallic to very light yellow-green
0.20 ₀		Light gold to yellow - slightly metallic
0.22 ₅		Gold with slight yellow-orange
0.25 ₀		Orange to melon
0.27 ₅		Red-violet
0.30 ₀		Blue to violet-blue
0.31 ₀		Blue
0.32 ₅		Blue to blue-green
0.34 ₅		Light green
0.35 ₀		Green to yellow-green
0.36 ₅	II	Yellow-green
0.37 ₅		Green-yellow
0.39 ₀		Yellow

Film Thickness (μ)	Order (5460 A)	Color and Comments
0.41 ₂		Light orange
0.42 ₆		Carnation pink
0.44 ₃		Violet-red
0.46 ₅		Red-violet
0.47 ₆		Violet
0.48 ₀		Blue-violet
0.49 ₃		Blue
0.50 ₂		Blue-green
0.52 ₀		Green (broad)
0.54 ₀		Yellow-green
0.56 ₀	III	Green-yellow
0.57 ₄		Yellow to "yellowish" (Not yellow but is in the position where yellow is to be expected. At times it appears to be light creamy grey or metallic.)
0.58 ₅		Light-orange or yellow to pink borderline
0.60 ₀		Carnation pink
0.63 ₀		Violet-red
0.68 ₀		"Bluish" (Not blue but borderline between violet and blue-green. It appears more like a mixture between violet-red and blue-green and overall looks greyish.)

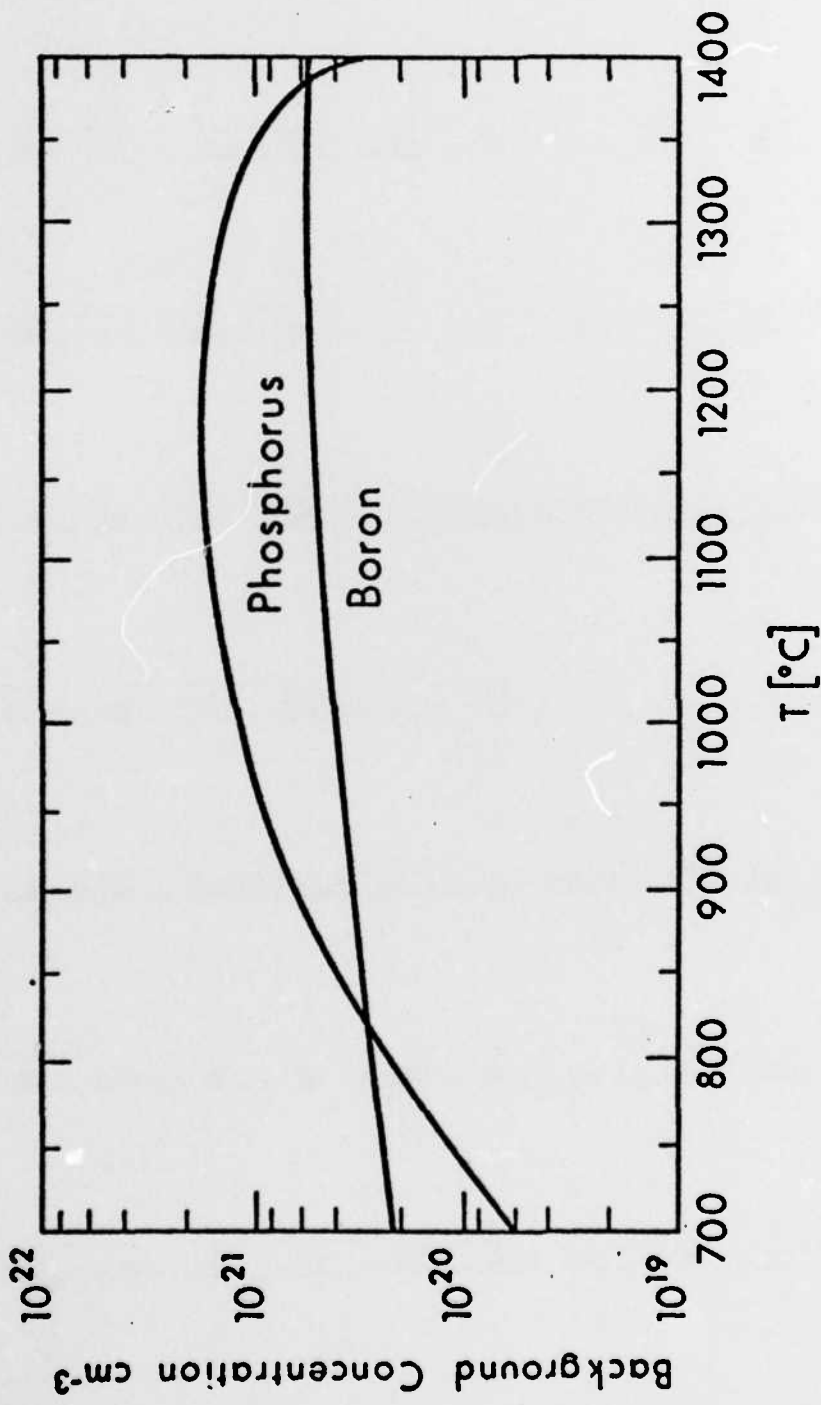
Film Thickness (μ)	Order (5460 Å)	Color and Comments
0.72	IV	Blue-green to green (quite broad)
0.77		"Yellowish"
0.80		Orange (rather broad for orange)
0.82		Salmon
0.85		Dull, light red-violet
0.86		Violet
0.87		Blue-violet
0.89		Blue
0.92	V	Blue-green
0.95		Dull yellow-green
0.97		Yellow to "yellowish"
0.99		Orange
1.00		Carnation pink
1.02		Violet-red
1.05		Red-violet
1.06		Violet
1.07		Blue-violet



Phosphorous diffusion coefficient as a function of temperature for silicon.⁴



Boron diffusion coefficient as a function of
temperature for silicon.⁴



Solid solubility of phosphorous and boron in silicon
as a function of temperature.⁵

REFERENCES

1. Burger, R. M. and R. P. Donovan, "Fundamentals of Silicon Integrated Device Technology," Vol. 1, Prentice Hall, Inc., Englewood Cliffs, NJ, 1967.
2. Deal, B. E., M. Sklar, A. S. Grove, and E. H. Snow, "Characteristics of the Surface State Charge (Q_{SS}) of Thermally Oxidized Silicon," J. Electrochemical Society, Vol. 113, March 1967.
3. Richman, P., "MOS Field-Effect Transistors and Integrated Circuits," John Wiley & Sons, New York, 1973.
4. Hamilton, D. J. and W. G. Howard, "Basic Integrated Circuit Engineering," McGraw-Hill Book Co., New York, New York, 1975.
5. Wolf, H. F., "Silicon Semiconductor Data," Pergamon Press, Elmsford, New York, 1969.
6. Muller, R. S. and T. I. Kamins, "Device Electronics for Integrated Circuits," John Wiley & Sons, New York, New York, 1977.
7. University of Hawaii. Physical Electronics Lab student handout. December 1977.

END

FILMED

9-83

DTIC

Background Concentration cm⁻³